nature portfolio

Peer Review File

Inhalable nanovesicles loaded with a STING agonist enhance CAR-T cell activity against solid tumors in the lung

Corresponding Author: Professor xi huang

Parts of this Peer Review File have been redacted as indicated to remove third-party material.

This file contains all reviewer reports in order by version, followed by all author rebuttals in order by version.

Version 0:

Reviewer comments:

Reviewer #1

(Remarks to the Author)
In this manuscript, Huang and colleagues utilized an anti-PD-L1-expressing nanovesicle loaded with cGAMP to potentiate CAR-T cell activity, a promising avenue in cancer immunotherapy. While the authors provided a substantial amount of data to support their findings, several key points require elucidation before publication:

1. Given the notably low loading efficiency of cGAMP (approximately 1‰), the authors should discuss the feasibility of future clinical translation and manufacturing.
2. The data depicted in Figure 4a are intriguing yet somewhat perplexing. Although the authors referenced "co-administration of aPD-L1 NVs and free STING agonists," Figure 4a only illustrates "NVs@cGAMP+ aPD-L1 NVs." The authors should explicate the results more clearly and elucidate the underlying mechanism, supported by references or relevant experiments.
3. In the in vivo antitumor experiments, the groupings fail to showcase the advantages of the inhalable drug delivery system adequately comparing with traditional administration route. Supplementing the groups with intravenous injection of aPD-L1 NVs@cGAMP and CAR-T cells is recommended.
4. The dosage in Figures 6a, 8a, and 8d should be described explicitly.
5. Regarding the mechanism by which NVs@cGAMP modulates the tumor microenvironment (TME) and prevents CAR-T cell exhaustion, the authors should furnish more comprehensive evidence and underscore the effect of nanovesicle carriers compared to other nanoparticles. For instance, they should investigate exhaustion markers of CAR-T cells.
6. The authors are encouraged to cite recent published papers on enhancing CAR-T therapy for solid tumors to provide a comprehensive overview of the field (e.g., Nat. Mater. https://doi.org/10.1038/s41563-024-01825-z, Nat. Biotechnol. https://doi.org/10.1038/s41587-023-02060-8 & https://doi.org/10.1038/s41587-023-02118-7, Nat. Rev. Bioeng. https://doi.org/10.1038/s44222-023-00148-z, Natl. Sci. Rev. https://doi.org/10.1093/nsr/nwae018).
7. Careful proofreading is advised to rectify typographical and grammatical errors in the manuscript. For instance, in Figure 1B, "MSLN" should be corrected to "MLSN." Additionally, clear differentiation between "NVs@cGAMP" and "aPD-L1 NVs@cGAMP" is essential.

Reviewer #2

(Remarks to the Author)
The manuscript by Zhu et al. (“Enhanced CAR-T cell activity against solid tumors by inhalable engineered nanovesicles”) describes the development and testing of an approach to treat lung cancer with a combination of CAR-T cells and PD-1L-targetd lipid vesicles that contain the STING agonist cGAMP. The paper is well written for the most part and contains a large quantity of supportive data. I do not see any experiments that could be added to complete what is already a quite thorough study.
Major points
1. The authors repeatedly state/imply that nanoparticles penetrate biological barriers well. Depending on their meaning of these statements, I take issue with such strong phrasing. It is not clear to me that nanoparticles penetrate biological barriers, other than via fusion and release of their contents into the cytoplasm. It is possible that some small fraction makes it through

the vessel wall by transcytosis, but this is also true for other large, hydrophilic entities. I would encourage the authors to be more explicit about the biophysical limitations of nanoparticles, targeted or not.

2. The translational relevance of many of these observations hangs on the mouse model. Although thoroughly characterized, one must question how relevant it is to the human disease. Again, there is not much that can be done to address such problems in the preclinical domain. However, I believe the authors should be more explicit about this issue, especially in this day and age where it is clear that many of the predictions based on these types of mouse models have not been born out in the clinic; this includes immuno-oncology models. An example of this kind of confusion is the line: "…but also highlight its role in inducing epitope spreading, which is critical for preventing tumor recurrence and enhancing the efficacy of CAR-T cell therapy." Epitope-spreading may be clear in mouse models, but is far from clear in human CAR-T therapy.
Minor points
1. Related to the point above, the authors should be clear about one obvious limitation of their B16 model. Though considered isogenic with C57/BL6, this cell line contains thousands of mutations, a significant fraction of which alter proteins. Thus, the immune system has much easier time recognizing its foreignness, being suddenly confronted by it, compared to the situation in human cancer.

2. This sentence is especially confusing and makes inconsistent claims: "These results suggest that the nebulized delivery of aPD-L1 NVs@cGAMP not only effectively overcome…"

3. A few figures/legends lack some important information; e.g., the Fig. 4 legend should clarify the times of the assays; Fig. 5 should include the quantification of (m).

Reviewer #3

(Remarks to the Author)
Dr. Tianchuan Zhu and colleagues have submitted a manuscript outlining their research on augmenting CAR-T cell activity against solid tumors using inhalable engineered nanovesicles. Their study suggests that inhaling an anti-PD-L1-expressing nanovesicle loaded with the STING agonist cGAMP could improve the effectiveness of CAR-T cells against solid tumors by reshaping the tumor microenvironment. However, I have identified several limitations outlined below, which currently impede a thorough understanding of the core concept and must be addressed to make a significant contribution to the field.

Major concerns：
1. In this study, the authors used a B16-grafted mouse model to represent metastatic lung cancer and tumor recurrence. However, it is noteworthy that B16 cells, as a melanoma cell line, do not accurately represent lung cancer. Consequently, the reliability of the results derived from this model in supporting the study's conclusions may be compromised. I recommend that the authors consider utilizing LLC cell line, a mouse Lewis lung cancer cell line, to establish a more pertinent mouse model for their research.

2. In this study, the authors assert that nanovesicles significantly improved the proliferation and antitumor effectiveness of CAR-T cells by restructuring the immunosuppressive tumor microenvironment. However, no evidence in figure 5 and figure 7 has been presented to support the claim that the immunosuppressive TME was effectively remodeled. I recommend that the authors provide substantial evidence or modify the statement regarding the effective remodeling of the immunosuppressive TME in order to validate their assertion.

3. In figure 2 k-m, the authors employed PBS as a control, which raises concerns about the robustness of the experimental setup. Given that the in vitro experiment used MOCK-T as a control, the authors need to use MOCK-T as a control instead of PBS as well, ensuring consistency across experiments. Moreover, the 14-day observation window is insufficient for a comprehensive evaluation of CAR-T cell efficacy. Additionally, it is crucial to display the percentages of T cells and CAR-T cells to demonstrate the expansion of CAR-T cells in the mice model.

4. In figures 3a-b, the level of green fluorescence alone may not be adequate to establish the expression of anti-PD-L1 scFv on 293T cells. Functional experiments should be conducted to bolster this claim. Furthermore, the method by which the authors measured the anti-PD-L1 scFv using flow cytometry was unclear; hence, additional experimental details must be included in the methods section.

5. In figure 3c, the authors used transmission electron microscopy to demonstrated that the aPD-L1 NVs were homogenous in structure. To make the results more convincing, the statistical analysis must be supplemented here.

6. In figure 3e, the methodology of detecting anti-PD-L1 scFv using an anti-PD-L1 antibody was not explicitly detailed. Therefore, it is essential to include experimental specifics in the methods section.

7. Figure 3l requires a negative control to demonstrate that nanovesicles can still induce IFN-β secretion from dendritic cells. Furthermore, the authors stated in lines 202-203 that their nanovesicles maintained the activity of the STING agonists, yet no evidence has been presented in their results to support STING activation. I recommend the authors to perform a Western Blot or another experiment to directly validate their conclusion.

8. In figure 4a, it would be valuable for the authors to provide an explanation as to why the co-administration of NVs@cGAMP and aPD-L1 NVs did not result in a significant increase in the IFN-β concentration. Additionally, the claim made by the authors regarding the co-administration of aPD-L1 NVs and free STING agonists not significantly increasing the IFN-β concentration in the supernatant (as mentioned in lines 217-218) should be aligned with the corresponding data in figure 4a. Furthermore, it would be of interest to elucidate the levels of other cytokines such as IFN-γ, IL-2, and TNF-α, to provide a more comprehensive understanding of the immune response elicited by the administered treatments. Clarifying these aspects will contribute to a more thorough interpretation of the results.

9. In figure 4c-f, the description concerning how the experiments were conducted remains unclear. In addition, the authors need to explain the rationale behind the inclusion of DCs in the co-culture system. They also need to provide detailed experimental procedures in the methods section.

10. The authors should provide an explanation on why both aPD-L1 NVs@cGAMP and free STING agonist treatments led to a significant upregulation of PD-L1 mRNA levels in tumor tissues (as depicted in figure 5d), while also enhancing the cytotoxicity of CAR-T cells (illustrated in figure 4e-f).

11. In lines 305-307, the authors asserted that aPD-L1 NVs@cGAMP demonstrate the ability to reverse immunosuppressive tumor microenvironments and inhibit metastatic growth in vivo. The authors should consider utilizing flow cytometry to assess specific immune cell populations, specifically targeting T cell subsets (including Th1, Th2, Th17, effector T cells, memory T cells, etc.), MDSCs, and other relevant markers associated with T cell exhaustion such as TIM3, LAG3, and TIGIT. This approach would facilitate the identification of any alterations within the immunosuppressive tumor microenvironment, offering valuable insights into the effects of the treatment.

12. In figure 6b, I recommend using nanovesicles without cGAMP as a control, as PBS alone is not sufficiently rigorous for this comparison. This adjustment is necessary because it ensures a more accurate evaluation of the specific impact attributed to the inclusion of cGAMP in the nanovesicles.

13. For all in vivo experiments in this study, the authors need to monitor and present the percentages of CAR-T cells at different time points. This practice ensures a comprehensive understanding of the persistence and behavior of CAR-T cells within the experimental model across the duration of the study.

14. In figures 6c, e, f, and g, it is recommended that the authors annotate the differences between the data and specify the statistical analysis methods used in the figure legends. This practice will enhance the comprehensibility of the experimental results and bolster their credibility.

15. In figure 7, the sole detection of M1 macrophages is insufficient to support a conclusion that the tumor microenvironment was changed. Additionally, it is advisable to charaterize M2 macrophages and other T cell subsets, and measure the levels of cytokines such as interleukin-10 and TGF-β. This approach will provide a more comprehensive evaluation of the immune landscape within the tumor microenvironment.

16. In lines 379-381, the author concluded that mature DCs activate CAR-T cells and support the development of long-term antitumor immune memory by presenting tumor antigens to T cells. However, there is a lack of correlated results to substantiate that the upregulation of CD80 and CD86 in DCs effectively activates CAR-T cells and promotes their long-term antitumor effect. Providing additional correlated data would strengthen the claim regarding the functional impact of mature DCs on CAR-T cell activation and long-term antitumor responses.

17. In lines 398-400, the author inferred that aPD-L1 NVs@cGAMP effectively reversed the immunosuppressive tumor microenvironment, rendering it proinflammatory and conducive to CAR-T cell proliferation and function. However, the evidences provided are not sufficient to support these conclusions. To substantiate the claim that the tumor microenvironment becomes proinflammatory, the authors should measure the levels of proinflammatory cytokines such as TNF-α, IL-6, and IL-1β within the tumor microenvironment. Furthermore, evaluating the presence and activation state of proinflammatory immune cells such as Th1 cells, cytotoxic T cells, and assessing the expression of inducible nitric oxide synthase (iNOS) and cyclooxygenase-2 (COX-2) would strengthen their case. Additionally, to demonstrate that CAR-T cell proliferation was enhanced, the percentage of CAR-T cells should be quantified. Incorporating these approaches will provide more robust evidence for the conclusions drawn.

18. In lines 413-416, the authors conclude that the resistance to B16 cells in CAR-T+NVs@cGAMP-cured mice could be attributed to an enhanced epitope spreading phenomenon. However, the results provided are not sufficient to support this conclusion. I suggest the authors consider conducting additional experiments or provide further analyses to substantiate this proposed mechanism. This may involve evaluating adaptive immune responses against a broader range of tumor antigens or conducting assays focused on epitope spreading to validate the proposed rationale.

19. In line 417 and line 430, the authors concluded that NVs@cGAMP enhanced CAR-T cell immune memory. I recommend that the authors detect the memory phenotype of CAR-T cells by using specific markers such as CD45RO, CD62L, and CCR7 to gain deeper insights into the memory T cell response. Incorporating these analyses will provide a more comprehensive validation of the impact of NVs@cGAMP on CAR-T cell immune memory.

Minor concerns:

1. In figure 2c, the authors utilized flow cytometry to quantify the CAR protein on the T cell surface. It is essential that the method for detecting the CAR protein on the T cell surface be thoroughly explained in the method section to ensure transparency and reproducibility of the experimental procedures.

2. In figure 2e-f, it would greatly improve the comparative analysis to display the statistical differences between each group, providing clearer insight into the observed variations.

3. In figure 1e, 1f, 1l, 1m, 2j, 5n, 6c, 6e, 6f, 8c and 8f, statistical analysis should be performed for comprehensive data evaluation.

4. In figure 8 and line 1017, the authors stated that all data are presented as mean ± S.D. However, it's important to highlight that only figure 8f follows this format. Therefore, I recommend revising line 1017 to ensure that the statement aligns with how the data are presented in the figure.

Reviewer #4

(Remarks to the Author)
In this study, the authors have designed a STING agonist (cGAMP) delivery strategy to improve CAR-T cell therapy. They used nanovesicles displaying anti-PDL-1 (aPDL-1-scFv) and loaded with STING agonist (cGAMP) as a strategy for this approach. They adopted intranasal delivery to target pulmonary immune responses, which could modulate immunosuppressive tumor microenvironment and enhance CAR-T cell accumulation in the tumor to improve therapeutic outcome. The study evaluated Mesothelin (MSLN) targeted CAR-T cells along with the aPDL-1 scFV engineered nanovesicle constructed from the cell membrane of 293T cells stably expressing aPD-L1-scFv for the study. The study initially evaluated MSLN-CAR-T against lung tumor developed using intravenous injection of B16-lung cancer cells and found a partial treatment response, which was further evaluated by combining with cGAMP loaded aPD-L1-NVs or as a mixture of cGAMP with aPD-L1-NVs with CAR-T cells to monitor the enhanced treatment outcome. The results found that when MSLN-CAR-T cells were combined with cGAMP loaded aPD-L1-NVs, the treatment outcome significantly improved. The study was well designed, and the results outcome are reasonably good but need further long-term validation to understand the potential application of this strategy to the next level in the clinic. There are several other important experiments need to be conducted to address for further validation of this research and treatment outcome. The manuscript can be considered for publication after addressing the following major concerns.
1. The measured zeta potential (Figure 3) of Free NVs is different from aPDL-1 NV. Please explain or perform another experiment where reconstruct Free NVs using aPD-L1 scFV and measure zeta potential. The expression of a single protein on the cell membrane will not provide this much change in the charge.
2. Figure 3l describing INF-beta secretion by DCs upon incubation with STING-NVs is misleading. The data does not explain what they have claimed in the manuscript.
3. STING agonist is important for activating immunosuppressive phenotype while aPD-L1-NV is important for blocking STING mediated upregulation of PD-L1 expression (Figure 4). This can happen either delivered using loaded NVs or STING+NV codelivery. What could be reason the codelivery is showing differential effect compared to loaded NVs? Please explain in the manuscript discussion.
4. Please explain in the results or figure legends the cell types used in each experiment. For example, cGAMP-NVs dose dependently enhance INF-beta secretion---in what cells. It would be easy for the readers to understand the results without going back and forth into the methods section.
5. The study claims that combination of aPD-L1 targeted cGAMP loaded NVs along with MSLN-CAR-T improves treatment outcome, but the survival curve results shows that only a slight improvement rather not achieving disease free outcome.
6. The entire study is conducted using a single B16 tumor model. It is better to address the efficacy of this treatment approach in another lung cancer model.
7. The endothelial anergy and tumor vascular expression of PD-L1 is linked with tumor targeted CAR-T and immune checkpoint blockade therapies. Please show some immunostaining results of lung tumor for vascular expression of PD-L1 after different treatments by co-staining with CD31 and PD-L1 targeted antibodies.
8. It is also important to show the amount of CAR-T cells presence after the completion of treatment to correlate the results with the treatment outcome in different groups by ex vivo histology of tumor and the spleen.
9. Figure 8, the tumor cell imaging immediately after implantation into inguinal region of the mouse is needed. The initial amount of implant is important for further tumor growth.

Version 1:

Reviewer comments:

Reviewer #1

(Remarks to the Author)
The authors have addressed my comments.

Reviewer #2

(Remarks to the Author)
he authors have done a decent job addressing my comments. I think the question of whether this type of preclinical study in the mouse, with its acknowledged limitations, is valuable enough to warrant publication in Nature Comm. is, it seems to me, an editorial decision.

Reviewer #3

(Remarks to the Author)
The authors have addressed most of my comments, but there are still some issues regarding rigor and unresolved mysteries in the manuscript.
Major comments
1. The authors have further demonstrated antitumor effects of MSLN CAR T cells in LLC tumor models. However, only four mice were used in the group infused with the CAR T cells in this experiment. In addition, the authors need to specify how many times the animal experiment has been repeated.

2. The authors suggested that CXCL9 and CXCL10 were upregulated in aPD-L1 NVs@cGAMP-MSLN CAR T cells. However, they did not characterize and provide evidence on whether these CAR T cells infiltrated into tumors, such as through IHC assays or immunofluorescence (IF).

3. The authors showed that treatment with aPD-L1 NVs@cGAMP increased the presence of T helper 1 (Th1) and Th17 cells, while reduced the number of Th2 cells in the tumor microenvironment (Fig. 5g and Fig. 5i). However, they did not explain why these changes happened. Were these phenotypes caused by the blockage of PD-L1 or TGF-β1? The authors should provide a discussion to clarify these results.
Minor comments
1. Please complete the unit information for the in vivo imaging figures.
2. The image data and corresponding statistical data are not presented together, making it difficult to read. The authors need to rearrange the layout of the images.
3. Please complete the statistical analysis of Supplementary Figure 12b, d, f.

Reviewer #4

(Remarks to the Author)
The revised manuscript by Zhu et al titled "Enhanced CAR-T cell activity against solid tumors by inhalable engineered nanovesicles" has extensively addressed to all the reviewers comments with a large number of additional experiments and with appropriate review of the previous literature to convincingly explain the background information needed for justifying the reviewers concerns. I am happy with the revision and can be now considered for publication.

Version 2:

Reviewer comments:

Reviewer #3

(Remarks to the Author)
The authors have addressed my points adequately.

Point-by-Point Response

NOTE: The comments are in italic black font, and our responses are in normal blue font. "Q" is short for "Question" and "R" is short for "Response".

Response to Comments from Reviewers

Reviewer #1 (Remarks to the Author): *with expertise in drug delivery, biomaterials, cancer therapy*

Q: *In this manuscript, Huang and colleagues utilized an anti-PD-L1-expressing nanovesicle loaded with cGAMP to potentiate CAR-T cell activity, a promising avenue in cancer immunotherapy. While the authors provided a substantial amount of data to support their findings, several key points require elucidation before publication:*

R: Thank you for your thoughtful evaluation and constructive suggestions. We deeply appreciate your effort in helping to enhance the quality of our manuscript. To address your concerns, we have diligently conducted extensive literature reviews and carried out additional experiments. Please find the following point-to-point responses to your comments and suggestions.

Q: *1. Given the notably low loading efficiency of cGAMP (approximately 1‰), the authors should discuss the feasibility of future clinical translation and manufacturing.*

R: Thank you for your insightful comments regarding the encapsulation (approximately 1‰, **Figure 3i**) and loading efficiency of cGAMP in our nanovesicles. Thanks to the enhanced delivery efficiency, cellular uptake and retention of cGAMP by aPD-L1 NVs, aPD-L1 NVs@cGAMP required only a very low dose of cGAMP to elicit a significant antitumor immune response.

However, as you have pointed out, improving the loading efficiency and encapsulation efficiency of cGAMP will help to improve the manufacturing efficiency and clinical translation of aPD-L1 NVs@cGAMP. In subsequent studies, we will try to change the conditions for loading STING agonists (e.g., increase the concentration of cGAMP, change the loading method) to improve the loading efficiency and encapsulation efficiency of cGAMP; in addition, we will also try to use fusion agents, enhance the electrostatic interaction between nanovesicles and cGAMP or promote the covalent linkage between the two, which will in turn improve the loading efficiency and encapsulation efficiency of cGAMP[1, 2, 3]. We believe that these improvements will help achieve GMP-compliant scale-up of aPD-L1 NVs@cGAMP.

We have included the corresponding discussion in the revised manuscript as follows:

(RES) need to be further addressed. In addition, aPD-L1 NVs@cGAMP required only 2% of the free STING agonist to induce a strong inflammatory immune response in tumor tissue and did not induce a systemic inflammatory response. However, it is important to acknowledge that the drug loading and encapsulation efficiencies of cGAMP in this study were relatively low. To improve the clinical translation and manufacturing feasibility of aPD-L1 NVs@cGAMP, further optimization of the drug loading conditions is necessary—such as increasing the concentration of cGAMP, altering the loading method, or adding fusion agents[74, 75]. Importantly, the results

Q: *2. The data depicted in Figure 4a are intriguing yet somewhat perplexing. Although the authors referenced "co-administration of aPD-L1 NVs and free STING agonists," Figure 4a only illustrates "NVs@cGAMP + aPD-L1 NVs." The authors should explicate the results more clearly and elucidate the underlying mechanism, supported by references or relevant experiments.*

R: Thank you for pointing out this important issue. We apologize for our carelessness that led to your confusion. In fact, we incorrectly wrote "cGAMP+ aPD-L1 NVs" (co-administration of aPD-L1 NVs and free STING agonists) as "NVs@cGAMP+ aPD-L1 NVs" in Figure 4a, Figure 4c, and Figure 4e. We have corrected "NVs@cGAMP+aPD-L1 NVs" to "cGAMP + aPD-L1 NVs" in the revised manuscript.

NVs@cGAMP was superior to the cGAMP + aPD-L1 NVs group in its ability to promote the release of inflammatory factors, possibly due to its enhanced cellular uptake and retention of STING agonists. In general, STING agonists that are hydrophilic and negatively charged have a poor ability to penetrate cell membranes and are therefore difficult to be taken up by cells; moreover, free STING agonists are degraded by phosphodiesterases in the circulation and on the cell surface, thus leading to a shorter half-life of STING agonists[4, 5, 6, 7]. In contrast, nanovesicles with lipid bilayers can rapidly enter the cell and facilitate cellular uptake of STING agonists. Kathleen M et al. demonstrated that cellular uptake of STING agonists loaded into extracellular vesicles was increased by approximately 10-fold compared to free STING agonists[8, 9].

We have included an interpretation of the results in the revised manuscript as follows:

TNF-α secretion enhancement. This synergistic effect may be attributed to aPD-L1 NVs facilitating the cellular uptake of STING agonists. Typically, STING agonists are hydrophilic and negatively charged, which limits their ability to penetrate cell membranes and results in poor cellular uptake[48, 49]. Moreover, free STING agonists are readily degraded by phosphodiesterases on the cell surface and in circulation, leading to a short half-life[50]. In contrast, nanovesicles with lipid bilayer structures can facilitate rapid entry into cells via endocytosis or membrane fusion, thereby improving the intracellular delivery and retention of STING agonists[51]. Studies by Kathleen M. et al. have demonstrated that loading STING agonists into extracellular vesicles increased cellular uptake tenfold compared to free STING agonists[49].

Q: *3. In the in vivo antitumor experiments, the groupings fail to showcase the advantages of the inhalable drug delivery system adequately comparing with traditional administration route. Supplementing the groups with intravenous injection of aPD-L1 NVs@cGAMP and CAR-T cells is recommended.*

R: Thank you for your constructive comments. In order to fully demonstrate the advantages of the inhaled drug delivery system, we supplemented the original subgroups with intravenous injection of aPD-L1 NVs@cGAMP and CAR-T cell groups, NVs@cGAMP (i. v.) + CAR-T. We have included the corresponding results in **Figures 6 and 7**, and the results are discussed in the revised manuscript.

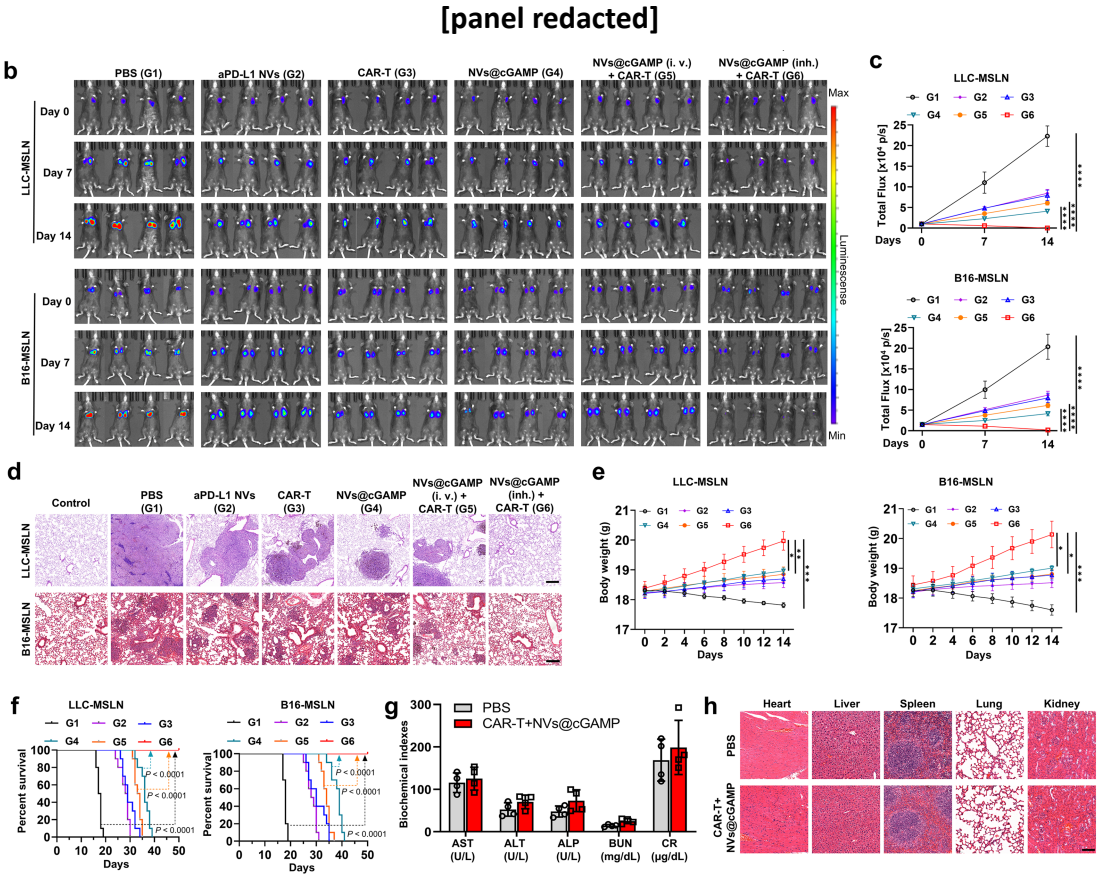

Figure 6. Enhancement of the antitumor capacity of CAR-T cells by aPD-L1 NVs@cGAMP.

(a) Schematic illustration of aPD-L1 NVs@cGAMP augmenting CAR-T cell anti-tumor efficacy. (b-c) Bioluminescence was measured by the IVIS system to evaluate tumor growth in the different treatment groups, and the bioluminescence intensity was statistically analyzed (n = 4). (d) Representative images of H&E-stained sections from LLC-MSLN and B16-MSLN tumor-bearing mice in various treatment groups. (e) Body weight change curves of mice treated with different agents in both tumor models (n = 4). (f) Survival curves of mice treated with different agents in both tumor models (n = 10). (g) Serum biochemical indices of mice receiving PBS or combined treatment with CAR-T cells and aPD-L1 NVs@cGAMP (n = 4). (h) Representative lung images and H&E-stained sections of mice receiving PBS or combined treatment with CAR-T cells and aPD-L1 NVs@cGAMP. Scale bar: 100 μm. All the data are presented as the mean ± S.D. *$p \leq 0.05$, **$p \leq 0.01$, ***$p \leq 0.001$ and ****$p \leq 0.0001$ by two-way ANOVA with Tukey's post-test for (c) and (e); and by log rank (Mantel-Cox) test for (f).

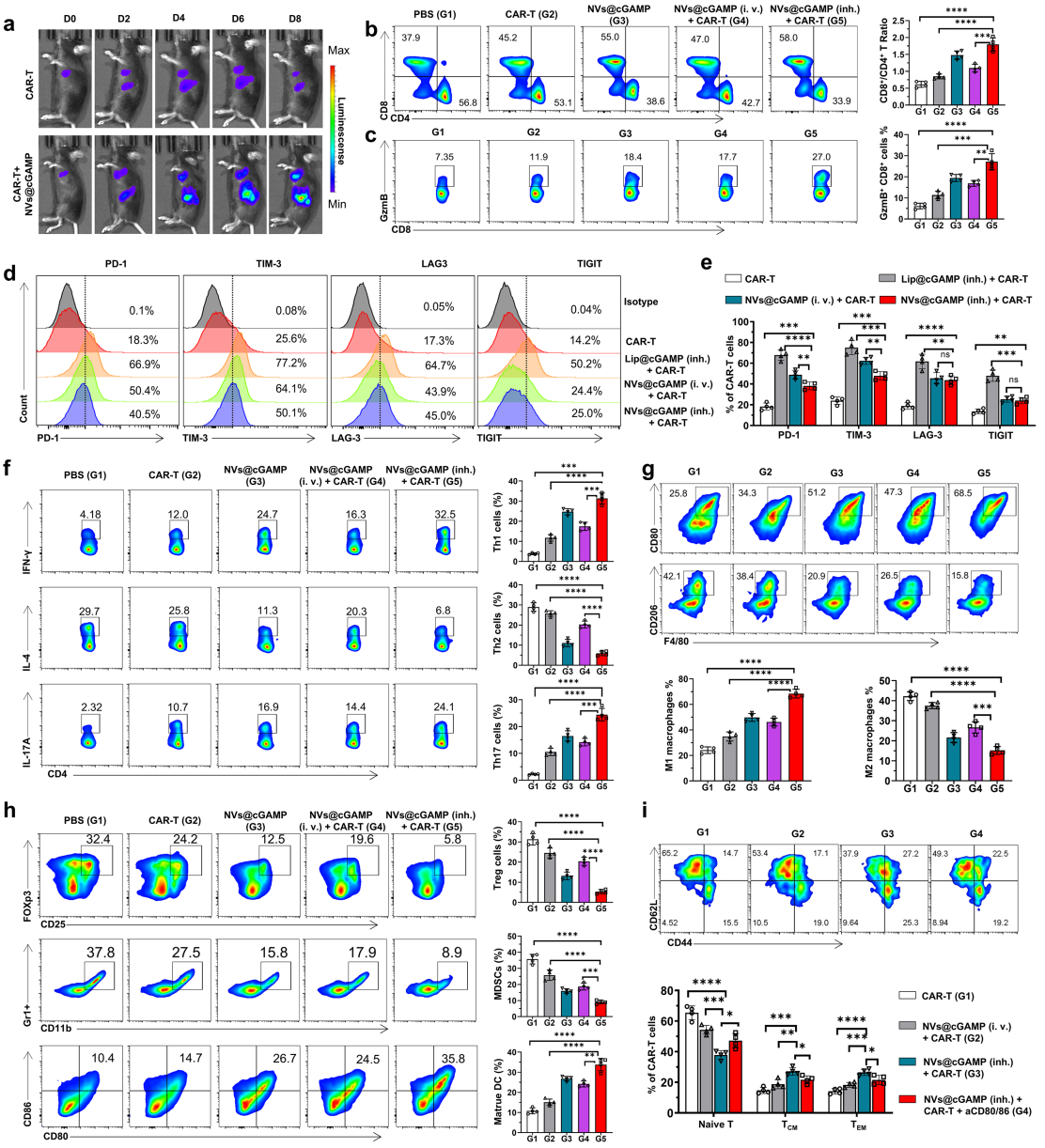

Figure 7. Changes in the tumor microenvironment after CAR-T+NVs@cGAMP treatment. (a) To assess the proliferation of CAR-T cells in different treatment groups, bioluminescence intensity was measured by IVIS at different time points after the injection of CAR-T cells expressing luciferase. (b-c) Representative flow cytometry plots and statistical analysis of (b) $CD8^+$ T cells and $CD4^+$ T cells and (c) infiltrating granzyme B-expressing $CD8^+$ T cells within the TME across various treatment groups (n = 4). (d-e) Representative flow cytometry plots and statistical analysis of T cell exhaustion markers (PD-1, TIM-3, LAG-3, TIGIT) on CAR-T within the TME across various treatment groups (n = 4). (f) Representative flow cytometry plots and statistical analysis of Th1, Th2 and Th17 within the TME across various treatment groups (n = 4). (g) Representative flow cytometry plots and statistical analysis of M1-type and M2-type macrophages within the TME across various treatment groups (n = 4). (h) Representative flow cytometry plots and statistical analysis of Tregs, MDSCs and mature DCs within the TME across various treatment groups (n = 4). (i) Representative flow cytometry plots and statistical analysis of naïve T cells, central memory T cells (T_{CM}), and effector memory T cells (T_{EM}) within the

CAR-T cell population in the TME across different treatment groups (n = 4). All the data are expressed as mean ± S.D. *$p \leq 0.05$, **$p \leq 0.01$, ***$p \leq 0.001$, ****$p \leq 0.0001$ and ns, not significant by one-way ANOVA with Tukey's post-test for (b)-(c) and (e)-(i).

Q: *4. The dosage in Figures 6a, 8a, and 8d should be described explicitly.*

R: Thank you for your suggestion. We have explicitly described the doses used in Figures 6a, 8a, and 8f (8d in the original manuscript) in the revised manuscript.

[figure redacted]

Figure 6. (a) Schematic illustration of aPD-L1 NVs@cGAMP augmenting CAR-T cell anti-tumor efficacy.

[figure redacted]

Figure 8. (a) Schematic illustration of the experimental design for evaluating anti-recurrence efficacy of MSLN CAR-T cells combined with NVs@cGAMP in LLC-MSLN and B16-MSLN tumor-bearing mice. (f) Schematic illustration of the evaluation of resistance to ectopic tumor recurrence after combined treatment with MSLN CAR-T cells and NVs@cGAMP.

Q: *5. Regarding the mechanism by which NVs@cGAMP modulates the tumor microenvironment (TME) and prevents CAR-T cell exhaustion, the authors should furnish more comprehensive evidence and underscore the effect of nanovesicle carriers compared to other nanoparticles. For instance, they should investigate exhaustion markers of CAR-T cells.*

R: We deeply appreciate your constructive comment. Per your suggestion, we evaluated markers of CAR-T cell exhaustion using flow cytometry (**Figure 7d-e**). Notably, we compared the effect of liposomes loaded with STING agonists (Lip@cGAMP) with NVs@cGAMP in preventing CAR-T cell exhaustion in this experiment. The exhaustion marker (PD-1, TIM-3, LAG3 and TIGIT) expression of CAR-T in the NVs@cGAMP + CAR-T cell group was significantly lower than that in the Lip@cGAMP + CAR-T cell group, which might be attributed to the blocking effect of anti-PD-L1 scFv on the surface of NVs@cGAMP on PD-L1.

In addition, in order to deeply investigate the mechanism by which NVs@cGAMP regulates the tumor microenvironment, we also evaluated the effects of NVs@cGAMP on cell subpopulations and cytokines in the tumor microenvironment. The results of flow cytometry showed that NVs@cGAMP increased the number of $CD8^+$ T cells, memory T cells, Th1, Th17, M1 and mature DCs, while decreasing the number of Treg, MDSC, M2 and Th2 cells in the tumor microenvironment. In addition, the results of ELISA showed that NVs@cGAMP promoted the levels of pro-inflammatory cytokines (IL-1β, IL-6, IL-7, IL-12, IL-15, and TGF-α) and decreased the levels of inhibitory cytokines (IL-10) in the tumor tissues.We have included the corresponding results in Figures 7, and the results are discussed in the revised manuscript.

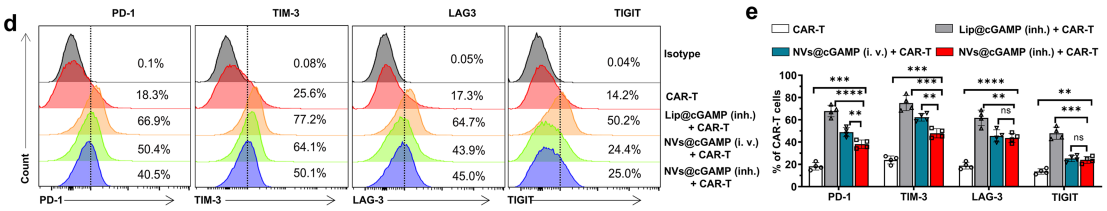

Figure 7. (d-e) Representative flow cytometry plots and statistical analysis of T cell exhaustion markers (PD-1, TIM-3, LAG-3, TIGIT) on CAR-T within the TME across various treatment groups (n = 4).

Q: *6. The authors are encouraged to cite recent published papers on enhancing CAR-T therapy for solid tumors to provide a comprehensive overview of the field (e.g., Nat. Mater. https://doi.org/10.1038/s41563-024-01825-z, Nat. Biotechnol. https://doi.org/10.1038/s41587-023-02060-8 & https://doi.org/10.1038/s41587-023-02118-7, Nat. Rev. Bioeng. https://doi.org/10.1038/s44222-023-00148-z, Natl. Sci. Rev. https://doi.org/10.1093/nsr/nwae018).*

R: Thank you for your recommendation. The five recommended articles on CAR-T therapy in solid tumor treatment have brought great inspiration to our research. We have cited these references in the revised manuscript (references 17, 18, 19, 36, 64).

Q: *7. Careful proofreading is advised to rectify typographical and grammatical errors in the manuscript. For instance, in Figure 1B, "MSLN" should be corrected to "MLSN." Additionally, clear differentiation between "NVs@cGAMP" and "aPD-L1 NVs@cGAMP" is essential.*

R: Thank you for your careful review. We have corrected "MLSN" in Figure 1B to "MSLN". In the original manuscript, we named the group of anti-PD-L1-expressing nanovesicle loaded with the STING agonist cGAMP as aPD-L1 NVs@cGAMP (or simply NVs@cGAMP), and the group that was treated with a combination of CAR-T cells and aPD-L1 NVs@cGAMP as the CAR-T+NVs@cGAMP group. To increase readability, we uniformly named the group of anti-PD-L1-expressing nanovesicle loaded with the STING agonist cGAMP as aPD-L1 NVs@cGAMP in the revised manuscript. Additionally, we have carefully checked the entire manuscript to avoid any grammatical or spelling errors.

Reviewer #2 (Remarks to the Author): *with expertise in CAR-T cells*

Q: *The manuscript by Zhu et al. ("Enhanced CAR-T cell activity against solid tumors by inhalable engineered nanovesicles") describes the development and testing of an approach to treat lung cancer with a combination of CAR-T cells and PD-1L-targetd lipid vesicles that contain the STING agonist cGAMP. The paper is well written for the most part and contains a large quantity of supportive data. I do not see any experiments that could be added to complete what is already a quite thorough study.*

R: Thank you very much for your positive comments and constructive suggestions. Please find the following point-to-point responses to your comments and suggestions.

Q: *1. The authors repeatedly state/imply that nanoparticles penetrate biological barriers well. Depending on their meaning of these statements, I take issue with such strong phrasing. It is not clear to me that nanoparticles penetrate biological barriers, other than via fusion and release of their contents into the cytoplasm. It is possible that some small fraction makes it through the vessel wall by transcytosis, but this is also true for other large, hydrophilic entities. I would encourage the authors to be more explicit about the biophysical limitations of nanoparticles, targeted or not.*

R: Thank you for your valuable suggestions. We fully appreciate your insightful comments regarding the terminology used to describe the ability of nanovesicles to penetrate biological barriers. In the revised manuscript, we have replaced the strong wording concerning the "penetration" capability of nanovesicles with more precise expressions.

Previous studies have shown that nanovesicles primarily deliver drugs to target cells through mechanisms such as membrane fusion, endocytosis (which includes phagocytosis, pinocytosis, and receptor-mediated endocytosis), and transcytosis. However, as you pointed out, while gene engineering techniques can enhance the targeting ability of nanovesicles, there are still numerous challenges in drug delivery based on their biophysical limitations:

(1) Surface Characteristics of Nanovesicles: The charge and surface proteins of nanovesicles can significantly influence their interactions with biological membranes. Although negatively charged nanovesicles may reduce clearance by the immune system, they may struggle to penetrate negatively charged tissues and cell membranes. Furthermore, certain proteins in the circulation can bind to the surface proteins of nanovesicles, leading to their clearance through opsonization[10, 11].

(2) Size of Nanovesicles: Smaller particles (approximately 50 nm) typically exhibit higher uptake rates, as they can navigate through narrow interstitial spaces and interact effectively with cell membranes via endocytosis. In contrast, larger particles (greater than 200 nm) may experience reduced permeability due to increased clearance by the mononuclear phagocyte system (MPS) and the reticuloendothelial system (RES). Therefore, a portion of nanovesicles may still be cleared by the RES system[12].

(3) Non-specific Distribution: While targeting ligands can enhance specificity towards target cells, there remains a risk of non-specific binding to healthy tissues or cells, which can lead to adverse side effects[12, 13].

(4) Drug Release from Nanovesicles: Currently, ensuring that nanovesicles release drugs at the correct time and location poses a challenge, particularly as nanovesicles may still be degraded by lysosomes after reaching the target site. Thus, further

improvements in the characteristics of nanovesicles are needed in subsequent studies to enhance drug delivery efficiency[10, 11, 14].

The biophysical limitations of nanovesicles have been discussed in our revised manuscript as follows:

> of STING agonists. However, it should be noted that nanovesicles as delivery vehicles also have their inherent biophysical limitations[51, 72, 73]. For instance, the negative charge on the surface of nanovesicles may weaken their fusion with cell membranes. Additionally, challenges such as non-specific distribution during administration, inability to precisely release drugs, and clearance by the reticuloendothelial system (RES) need to be further addressed. In addition, aPD-L1 NVs@cGAMP required only

Thank you for your constructive feedback, which has greatly improved the quality of our work.

Q: *2. The translational relevance of many of these observations hangs on the mouse model. Although thoroughly characterized, one must question how relevant it is to the human disease. Again, there is not much that can be done to address such problems in the preclinical domain. However, I believe the authors should be more explicit about this issue, especially in this day and age where it is clear that many of the predictions based on these types of mouse models have not been born out in the clinic; this includes immuno-oncology models. An example of this kind of confusion is the line: "…but also highlight its role in inducing epitope spreading, which is critical for preventing tumor recurrence and enhancing the efficacy of CAR-T cell therapy." Epitope-spreading may be clear in mouse models, but is far from clear in human CAR-T therapy.*

R: We fully agree with your suggestion. The use of mouse models in immuno-oncology research provides valuable insights into potential therapeutic strategies, but has significant limitations in predicting therapeutic outcomes in human patients. These limitations include, but are not limited to:

(1) Genetic and physiological differences: Mice and humans have significant genetic, immunological and physiological differences, and most preclinical studies use inbred mouse strains, resulting in genetically homogeneous populations[15];

(2) Differences in the tumor microenvironment: mouse models often do not accurately represent the complex interactions within the TME found in humans; in addition, mice grown under pathogen-free (SPF) conditions have large differences in immune system development compared to humans exposed to a variety of pathogens[15];

(3) Differences in timing of interventions: in mouse models, interventions are often performed soon after tumor implantation, whereas in human patients, interventions

are often performed in mid- to late stage, after immune evasion mechanisms have been established[16].

(4) Differences in epitope spreading: the B16 tumor model has limitations in generalizing the findings to human cancer immunotherapy due to the large differences in mutation load, MHC class I expression levels, and the tumor microenvironment, and subsequent more complex models are needed to fully understand the epitope spreading phenomenon[17, 18].

To emphasize the uncertainty of translating the results obtained in mouse models to the clinic, we have changed the original statementto the following in the revised manuscript :

These results not only confirmed that CAR-T+NVs@cGAMP reversed the tumor microenvironment, but also highlighted its role in inducing epitope spreading in mouse tumor models. However, considering that the B16 and LLC models are quite different from human tumor patients in terms of tumor heterogeneity and tumor microenvironment, subsequent validation of these results in more complex models is needed, which is crucial for the future use of NVs@cGAMP to prevent tumor recurrence and improve the efficacy of CAR-T cell therapy[58, 59, 60, 61].

Q: *Minor points:1. Related to the point above, the authors should be clear about one obvious limitation of their B16 model. Though considered isogenic with C57/BL6, this cell line contains thousands of mutations, a significant fraction of which alter proteins. Thus, the immune system has much easier time recognizing its foreignness, being suddenly confronted by it, compared to the situation in human cancer.*

R: Thank you for pointing out the limitations of the B16 tumor model in assessing efficacy. Although the B16 tumor model has been widely used to assess the efficacy of a variety of drugs, there are still many limitations, including: (1) Immunogenicity of mutations: many non-synonymous mutations in B16F10 cells can lead to the production of novel peptides that can be recognized by $CD8^+$ T cells, and the immune system recognizes and responds to these mutant proteins with the potential to enhance anti-tumor immunity in the organism[19, 20]; (2) Lack of genetic complexity: B16 tumors lack the genetic complexity and heterogeneity seen in human melanomas. They typically harbor a single driver mutation (BRAF V600E) and do not accumulate additional mutations over time[16, 18]; (3) Differences in tumor architecture and microenvironment: B16 tumors grown in mice do not fully recapitulate the 3D structure and heterogeneity of human melanomas[15, 17].

Following your suggestions, we have analyzed the limitations of the B16 tumor model in detail in the revised manuscript, and we emphasize the need for future studies using other models to confirm our findings.

Q: *Minor points: 2. This sentence is especially confusing and makes inconsistent claims: "These results suggest that the nebulized delivery of aPD-L1 NVs@cGAMP not only effectively overcome…"*

R: Thank you very much for pointing this out. Here is an explanation of the statement:

Previous studies have shown that while STING agonists can directly activate T cells, excessive intake can lead to T cell exhaustion[9]. However, due to the low cell permeability and tissue retention of conventional STING agonists, high doses of STING agonists often need to be injected to achieve the necessary exposure in the TME to activate antigen presenting cells[4, 8]. Therefore, we expect that STING agonists will be more readily taken up by DCs and tumor cells to achieve this delicate balance between effective immune stimulation and T cell exhaustion. In the present study, aPD-L1 NVs@cGAMP promoted better uptake of STING agonists by DCs and tumor cells, thereby activating the body's anti-tumor immune response at a very low dose and avoiding the T-cell exhaustion associated with the use of high-dose STING agonists.

To make our point clearer, we have changed the original sentence to read as follows:

"These results suggest that nebulized delivery of aPD-L1 NVs@cGAMP effectively overcomes the problems of low cell permeability and poor tissue retention of STING agonists, and can activate the body's antitumor immune response at a low dose of STING agonists. Therefore, aPD-L1 NVs@cGAMP reduces the nonspecific uptake of STING agonists by T cells to a certain extent, and avoids T cell exhaustion caused by T cell uptake of high doses of STING agonists."

Q: *Minor points: 3. A few figures/legends lack some important information; e.g., the Fig. 4 legend should clarify the times of the assays; Fig. 5 should include the quantification of (m).*

R: Thanks for your suggestions. In the revised manuscript, we have added the time of analysis to the legend of Figure 4 and quantified the bioluminescence intensity in Figure 5m.

Reviewer #3 *(Remarks to the Author): with expertise in CAR-T cells*

Q: *Dr. Tianchuan Zhu and colleagues have submitted a manuscript outlining their research on augmenting CAR-T cell activity against solid tumors using inhalable engineered nanovesicles. Their study suggests that inhaling an anti-PD-L1-expressing nanovesicle loaded with the STING agonist cGAMP could improve the effectiveness of CAR-T cells against solid tumors by reshaping the tumor microenvironment. However, I have identified several limitations outlined below, which currently impede a thorough understanding of the core concept and must be addressed to make a significant contribution to the field.*

R: Thank you for your thoughtful evaluation and constructive suggestions. We deeply appreciate your efforts in improving the quality of our manuscript. To address your concerns, we have carefully reviewed the relevant literature and conducted additional experiments to strengthen our findings. Specifically, we have re-evaluated the efficacy of our therapeutic strategy using the Lewis Lung Carcinoma (LLC) model. We highly value your expertise, and should there be any additional points requiring our attention, we stand ready to make necessary revisions. Please find the following point-to-point responses to your comments and suggestions.

Q: *1. In this study, the authors used a B16-grafted mouse model to represent metastatic lung cancer and tumor recurrence. However, it is noteworthy that B16 cells, as a melanoma cell line, do not accurately represent lung cancer. Consequently, the reliability of the results derived from this model in supporting the study's conclusions may be compromised. I recommend that the authors consider utilizing LLC cell line, a mouse Lewis lung cancer cell line, to establish a more pertinent mouse model for their research.*

R: We sincerely appreciate your insightful suggestion. Indeed, Reviewer 4 also recommended incorporating an additional tumor model alongside the B16 model to evaluate the efficacy of our cancer treatment strategy more comprehensively. As you correctly pointed out, B16 cells are a melanoma cell line, and the B16 metastatic lung cancer model primarily represents metastatic lung cancer originating from other tissues. However, lung cancer encompasses both metastatic lung cancer and primary lung cancer arising from lung tissue itself. In our original manuscript, the use of the B16 tumor model only reflected the efficacy of our strategy against metastatic lung tumors.

To address this limitation and in accordance with your recommendation, we have established an LLC (Lewis Lung Carcinoma) tumor model to assess the effectiveness of our strategy on primary lung tumors. In the revised manuscript, we have utilized the LLC tumor model as the primary model to evaluate our strategy's efficacy, while retaining the B16 tumor model as a supplementary model to demonstrate the treatment's versatility against metastatic tumors. This dual-model approach allows us to present a more robust evaluation of our therapy's potential in both primary and metastatic contexts.

We have significantly updated the figures and reorganized the results to reflect these additions. Specifically, we have incorporated the findings from the LLC tumor model into **Figures 2, 5, 6, 7, and 8**, and have provided a detailed discussion of the corresponding results.

Thank you once again for your valuable feedback. Your suggestion has significantly improved the quality and relevance of our study.

Q: *2. In this study, the authors assert that nanovesicles significantly improved the proliferation and antitumor effectiveness of CAR-T cells by restructuring the immunosuppressive tumor microenvironment. However, no evidence in figure 5*

and figure 7 has been presented to support the claim that the immunosuppressive TME was effectively remodeled. I recommend that the authors provide substantial evidence or modify the statement regarding the effective remodeling of the immunosuppressive TME in order to validate their assertion.

R: Thank you for your insightful suggestion. We fully agree that our original assertion—that nanovesicles can effectively remodel the immunosuppressive tumor microenvironment—requires more substantial evidence.

Based on your recommendation, we have toned down this statement throughout the manuscript. Additionally, inspired by your subsequent detailed and constructive comments, we have conducted additional experiments to provide more evidence supporting this assertion. Specifically, following your recommendations in comments 11, 15, and 17, we have:

(1) Flow Cytometry Analyses (Figures 5 and 7): We analyzed T cell subsets (including Th1, Th2, Th17, effector T cells, and memory T cells) and T cell exhaustion markers (PD-1, TIM-3, LAG-3, and TIGIT). We also evaluated the memory phenotypes of CAR-T cells, as well as the populations of Tregs, MDSCs, and macrophage polarization (M1 and M2).

(2) Cytokine Profiling via ELISA (Fig. 5a and Supplementary Figure 26):We measured the secretion levels of pro-inflammatory cytokines (TNF-α, IL-6, IL-7, IL-12, IL-15, IL-1β, IFN-γ, IFN-β) and anti-inflammatory cytokines (IL-10 and TGF-β) within the tumor microenvironment.

(3) Immunohistochemistry Assessments (Supplementary Figure 24): We evaluated the expression levels of inducible nitric oxide synthase (iNOS) and cyclooxygenase-2 (COX-2) to further understand the inflammatory status of the tumor microenvironment.

While these additional experiments may not completely prove that nanovesicles have remodeled the immunosuppressive TME, it does demonstrate their significant potential in reshaping the tumor environment.

We sincerely appreciate your detailed and constructive suggestions. Your comments has enabled us to provide more substantial evidence and a clearer understanding of how nanovesicles may contribute to remodeling the TME and enhancing the efficacy of CAR-T cell therapy in tumor immunotherapy.

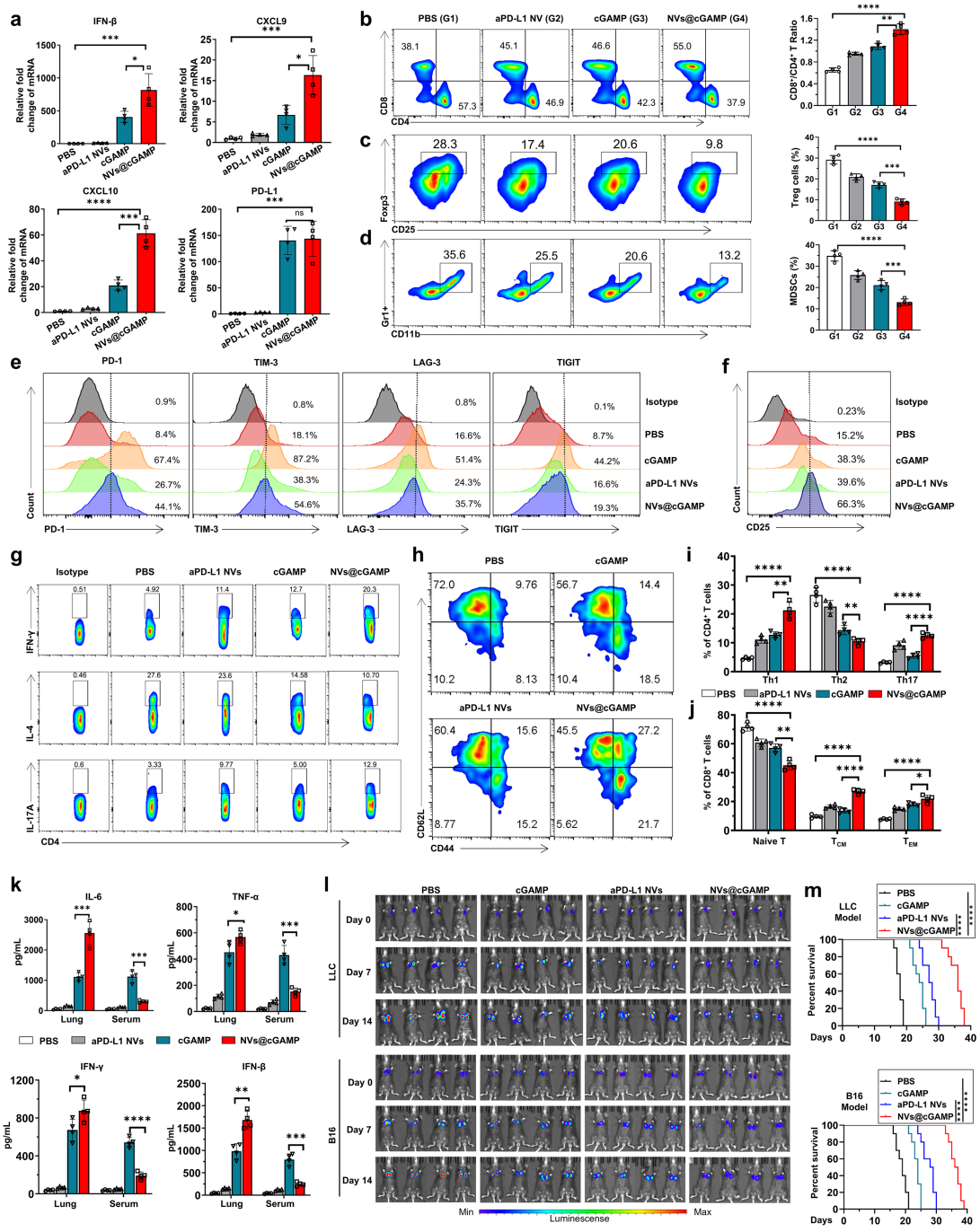

Figure 5. Remodeling of the tumor microenvironment and inhibition of tumor growth by aPD-L1 NVs@cGAMP. (a) Changes in the gene expression levels of IFN-β, CXCL9, CXCL10, and PD-L1 in tumor tissues of LLC-MSLN tumor-bearing mice after inhalation of the different agents (n = 4). (b-d) Representative flow cytometry plots and statistical analysis of (b) $CD8^+$ T cells and $CD4^+$ T cells, (c) Treg cells and (d) MDSCs within the TME across various treatment groups (n = 4). (e) Analysis of T cell exhaustion markers PD-1, TIM-3, LAG-3, and TIGIT in different treatment groups by flow cytometry. (f) Expression levels of CD25 on T cells in different treatment groups, analyzed by flow cytometry. (g, i) Representative flow cytometry plots and statistical analysis of Th1, Th2, and Th17 cells within the TME across different treatment groups (n = 4). (h, j) Representative flow cytometry plots and statistical analysis of

naïve T cells, central memory T cells (T_{CM}), and effector memory T cells (T_{EM}) within the TME across different treatment groups (n = 4). (k) Concentrations of IL-6, TNF-α, IFN-γ and IFN-β in the lung tissue and serum of mice after inhalation of different agents (n = 4). (l) Bioluminescence measured by an IVIS system for assessment of tumor growth after administration of different agents to tumor-bearing mice. (m) Survival curves of tumor-bearing mice treated with different agents (n = 10). All data are presented as the mean ± S.D. *$p \leq 0.05$, **$p \leq 0.01$, ***$p \leq 0.001$, ****$p \leq 0.0001$ and ns, not significant by one-way ANOVA with Tukey's post-test for (a), (b), (i) and (j); by Student's t test for (k); and by log rank (Mantel-Cox) test for (m).

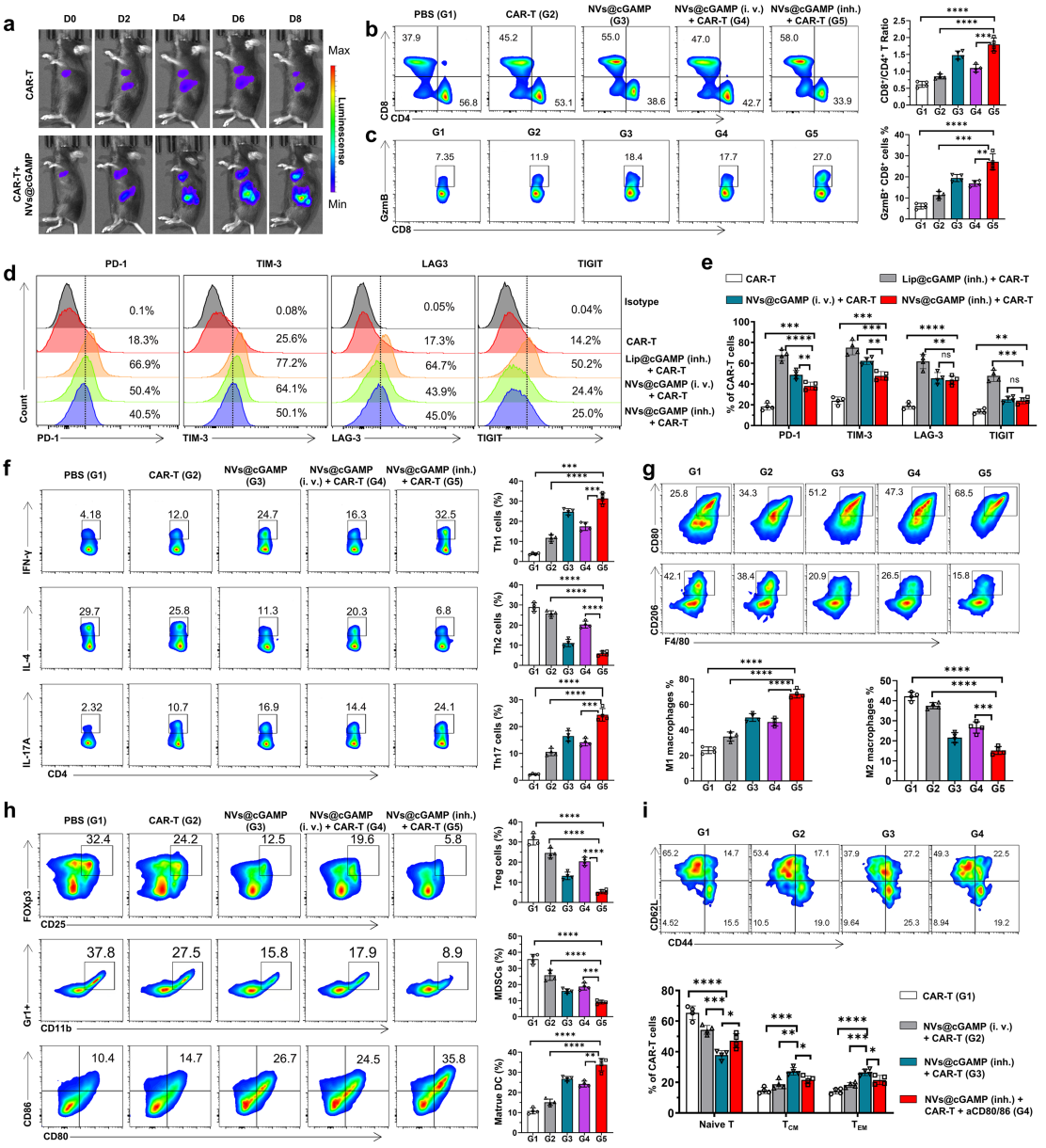

Figure 7. Changes in the tumor microenvironment after CAR-T+NVs@cGAMP treatment. (a) To assess the proliferation of CAR-T cells in different treatment groups, bioluminescence intensity was measured by IVIS at different time points after the injection of CAR-T cells expressing luciferase. (b-c) Representative flow cytometry plots and statistical analysis of (b) $CD8^+$ T cells and $CD4^+$ T cells and (c) infiltrating granzyme B-expressing $CD8^+$ T cells within

the TME across various treatment groups (n = 4). (d-e) Representative flow cytometry plots and statistical analysis of T cell exhaustion markers (PD-1, TIM-3, LAG-3, TIGIT) on CAR-T within the TME across various treatment groups (n = 4). (f) Representative flow cytometry plots and statistical analysis of Th1, Th2 and Th17 within the TME across various treatment groups (n = 4). (g) Representative flow cytometry plots and statistical analysis of M1-type and M2-type macrophages within the TME across various treatment groups (n = 4). (h) Representative flow cytometry plots and statistical analysis of Tregs, MDSCs and mature DCs within the TME across various treatment groups (n = 4). (i) Representative flow cytometry plots and statistical analysis of naïve T cells, central memory T cells (T_{CM}), and effector memory T cells (T_{EM}) within the CAR-T cell population in the TME across different treatment groups (n = 4). All the data are expressed as mean ± S.D. *$p \leq 0.05$, **$p \leq 0.01$, ***$p \leq 0.001$, ****$p \leq 0.0001$ and ns, not significant by one-way ANOVA with Tukey's post-test for (b)-(c) and (e)-(i).

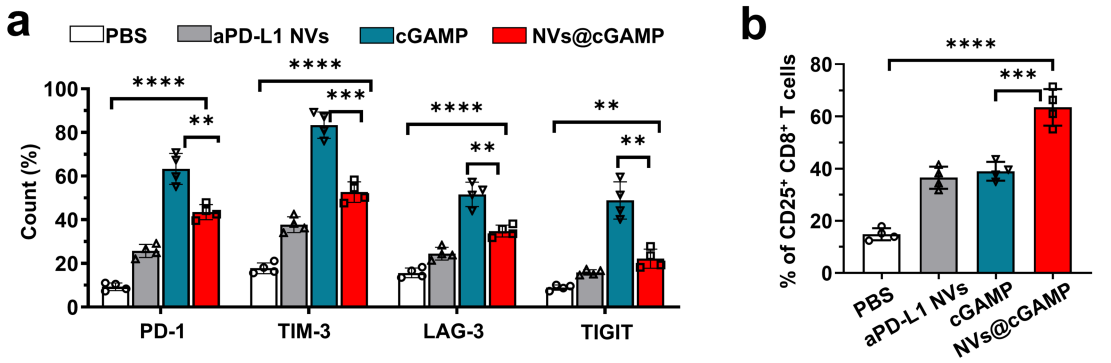

Supplementary Figure 14. (a) Statistical analysis of T cell exhaustion markers PD-1, TIM-3, LAG-3, and TIGIT across different treatment groups (n = 4). (b) Statistical analysis of CD25 expression levels on T cells across different treatment groups (n = 4). **$p \leq 0.01$, ***$p \leq 0.001$, ****$p \leq 0.0001$ by one-way ANOVA with Tukey's post-test for (a) and (b).

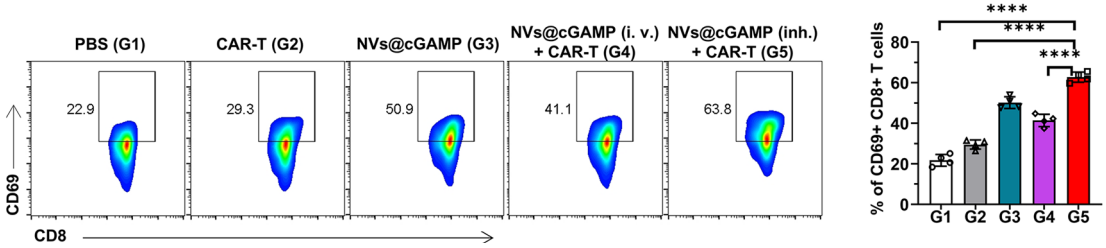

Supplementary Figure 23. Representative flow cytometry plots and statistical analysis of CD69 expression on T cells within the TME across various treatment groups (n = 4). Data are presented as the mean ± S.D. ****$p \leq 0.0001$ by one-way ANOVA with Tukey's post-test.

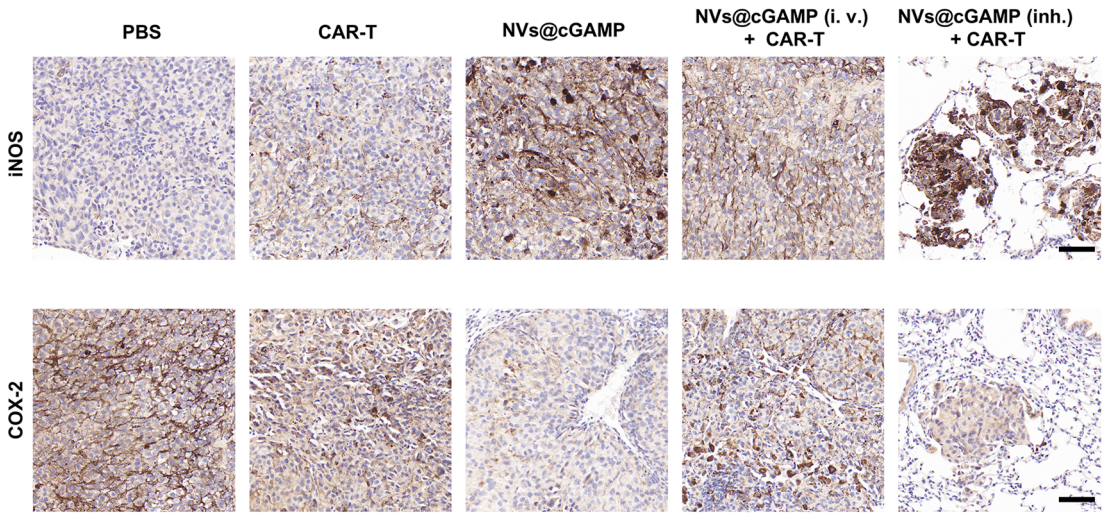

Supplementary Figure 24. Expression of iNOS and COX-2. LLC-MSLN tumor-bearing mice receiving different treatments were assessed for iNOS and COX-2 expression in tumor tissues via immunohistochemistry. Scale bar: 200 μm..

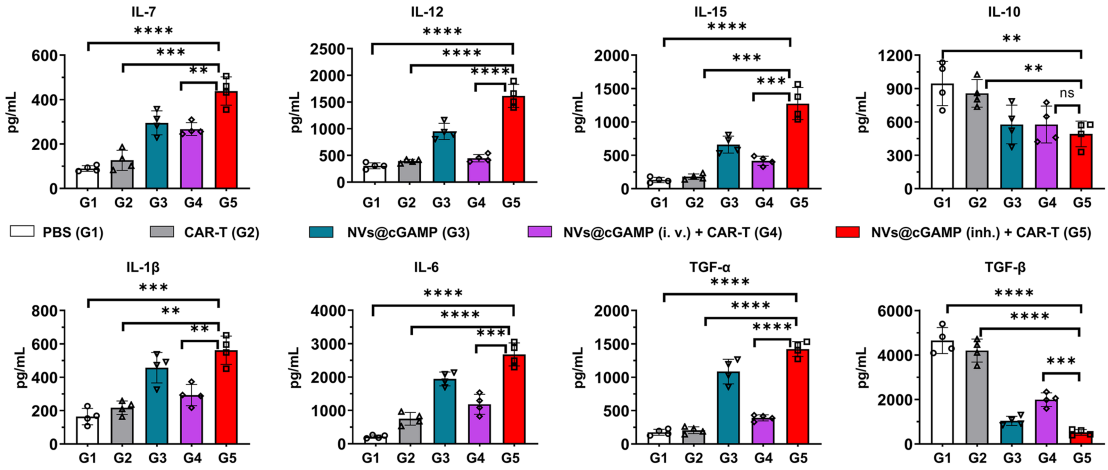

Supplementary Figure 26. Cytokine concentrations of IL-7, IL-12, IL-15, IL-10, IL-1β, IL-6, TGF-α and TGF-β in tumor tissue homogenates from different treatment groups were quantified by ELISA (n = 4). Data are presented as the mean ± S.D. $^{**}p \leq 0.01$, $^{***}p \leq 0.001$, $^{****}p \leq 0.0001$ by one-way ANOVA with Tukey's post-test.

Q: *3. In figure 2 k-m, the authors employed PBS as a control, which raises concerns about the robustness of the experimental setup. Given that the in vitro experiment used MOCK-T as a control, the authors need to use MOCK-T as a control instead of PBS as well, ensuring consistency across experiments. Moreover, the 14-day observation window is insufficient for a comprehensive evaluation of CAR-T cell efficacy. Additionally, it is crucial to display the percentages of T cells and CAR-T cells to demonstrate the expansion of CAR-T cells in the mice model.*

R: Thank you for your insightful suggestions. We have replaced PBS with MOCK-T cells as the control in Figure 2k-m to ensure consistency across our experiments. Additionally, we have extended the observation period to 21 days to provide a more

comprehensive evaluation of CAR-T cell efficacy. We also collected peripheral blood samples from mice at various time points *via* tail vein sampling and used flow cytometry to assess the percentages of MOCK-T cells and CAR-T cells. These results have been incorporated into **Figure 2k-m** and **Supplementary Fig. 7** and are discussed in the revised manuscript. The updated figures are provided below:

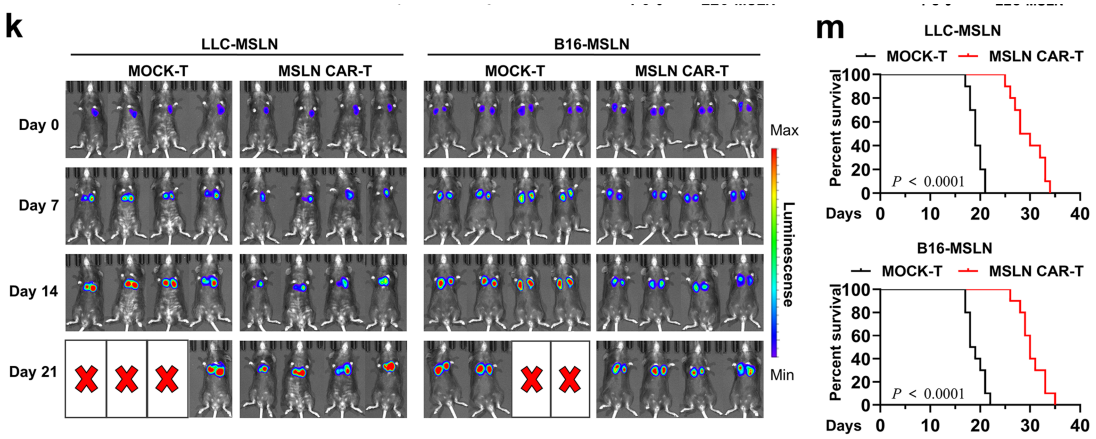

Figure 2. (k) Antitumor effects of CAR-T cells on LLC-MSLN and B16-MSLN tumor-bearing mice was evaluated using the IVIS system after injection of MOCK-T cells or MSLN CAR-T cells (n = 4). (m) Survival curves of LLC-MSLN and B16-MSLN tumor-bearing mice after injection of MOCK-T cells or MSLN CAR-T cells (n = 10).

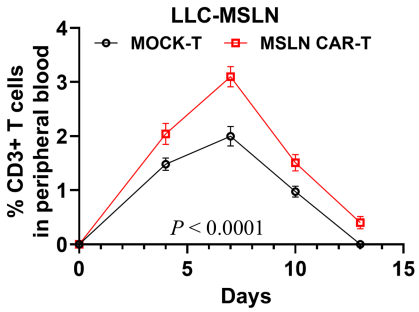

Supplementary Fig. 7. Following injection of GFP-expressing MOCK-T or MSLN CAR-T cells into LLC-MSLN tumor-bearing mice, flow cytometry was used to analyze the percentage of CAR-T cells in peripheral blood at various time points (n = 4). ****$p \leq 0.0001$ by two-way ANOVA with Tukey's post-test.

Q: *4. In figures 3a-b, the level of green fluorescence alone may not be adequate to establish the expression of anti-PD-L1 scFv on 293T cells. Functional experiments should be conducted to bolster this claim. Furthermore, the method by which the authors measured the anti-PD-L1 scFv using flow cytometry was unclear; hence, additional experimental details must be included in the methods section.*

R: Thank you for your valuable suggestion. While we initially characterized the overexpression of anti-PD-L1 scFv on 293T cells (aPD-L1 293T) using inverted fluorescence microscopy and flow cytometry, we agree that additional functional

experiments are essential to robustly confirm the successful expression of anti-PD-L1 scFv on these cells.

To address this concern, we conducted *in vitro* binding assays to evaluate the functional expression of anti-PD-L1 scFv on aPD-L1 293T cells by assessing their ability to bind recombinant PD-L1 protein. Specifically, we prepared 293T cells stably expressing only GFP (293T-GFP) as a control. Both 293T-GFP and aPD-L1 293T cells were incubated with 10 μg/mL recombinant PD-L1 protein for 4 hours. After washing away unbound PD-L1 protein, the cells were stained with Alexa Fluor® 647-labeled anti-PD-L1 antibody and examined using confocal microscopy. As shown in **Supplementary Fig. 8**, no red fluorescence was observed around the 293T-GFP cells, indicating negligible binding of PD-L1 protein. In contrast, significant red fluorescence was detected around aPD-L1 293T cells, demonstrating that the anti-PD-L1 scFv expressed on these cells is functionally capable of binding PD-L1 protein.

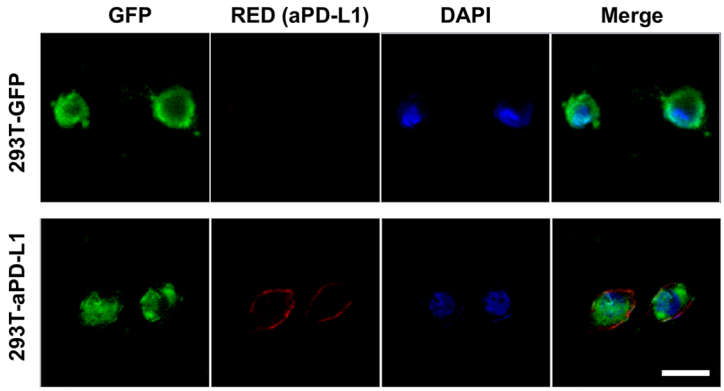

Supplementary Fig. 8. Binding of 293-aPD-L1 cells to recombinant PD-L1 protein. After co-incubation of 293-aPD-L1 cells with recombinant PD-L1 protein, the cells were stained using an anti-PD-L1 antibody, and binding interactions were assessed *via* confocal microscopy. Scale bar: 20 μm.

Additionally, we have included detailed descriptions of the methods used to detect anti-PD-L1 scFv expression in the revised manuscript, as follows:

"**Characterization of anti-PD-L1 scFv expression in aPD-L1 293T cells and nanovesicles**

In this study, we employed Protein L to detect the presence of anti-PD-L1 scFv on the surfaces of aPD-L1 293T cells and aPD-L1 NVs. Protein L specifically binds to the κ light chain of the scFv region, making it an effective tool for detecting scFv fragments and chimeric antigen receptors (CARs) expressed on cell membranes. To detect anti-PD-L scFv on the surface of aPD-L1 293T cells, we incubated 1×10^6 cells with 1 μL Protein L (1 mg/mL) at 4 °C for 30 minutes, followed by washing with PBS. The cells were then stained with PE-conjugated streptavidin (BioLegend, San Diego, CA, USA) and analyzed using a CytoFLEX LX flow cytometer (Beckman Coulter, Atlanta, GA, USA).

To facilitate the detection of anti-PD-L1 scFv on NVs, we incubated 20 μL of nanovesicles with 10 μL of 4 μm aldehyde/sulfate latex beads (Invitrogen) at room temperature for 15 minutes. We then added 1 mL PBS and rotated the mixture for 2 hours to allow efficient coupling of the nanovesicles to the beads. After adding 110 μL glycine (100 mM) and incubating for 30 minutes, the bead-bound nanovesicles were collected by centrifugation. The samples were then stained with Protein L and PE-conjugated streptavidin as described above and analyzed by flow cytometry."

Q: *5. In figure 3c, the authors used transmission electron microscopy to demonstrated that the aPD-L1 NVs were homogenous in structure. To make the results more convincing, the statistical analysis must be supplemented here.*

R: Thank you for your valuable suggestion. In accordance with your recommendation, we have conducted a statistical analysis of the particle size distribution of the aPD-L1 nanovesicles observed in the TEM images. We have incorporated this data into **Supplementary Fig. 9** of the revised manuscript to strengthen the validity of our results.

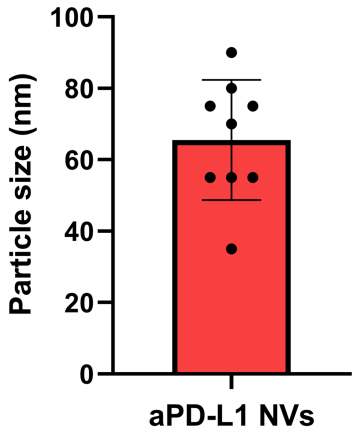

Supplementary Fig. 9. Statistical analysis of the size distribution of aPD-L1 NVs obtained through transmission electron microscopy (n = 9).

Q: *6. In figure 3e, the methodology of detecting anti-PD-L1 scFv using an anti-PD-L1 antibody was not explicitly detailed. Therefore, it is essential to include experimental specifics in the methods section.*

R: Thank you for your valuable suggestion. We have added detailed experimental procedures for detecting the expression of anti-PD-L1 scFv in nanovesicles and cells using Western blotting to the Methods section of the revised manuscript. The added details are as follows:

"Western blot analysis was performed to detect the expression of the anti-PD-L1 scFv protein in engineered 293T cells and nanovesicles. In this study, the anti-PD-L1 scFv protein was tagged with a Myc epitope tag, enabling detection using an anti-Myc monoclonal antibody. Briefly, cells and nanovesicles were lysed using RIPA buffer before the total protein concentration was determined using a BCA protein assay kit

(Pierce, USA). After equal amounts of proteins were separated and transferred to polyvinylidene difluoride (PVDF) membranes *via* 10% SDS–PAGE, the PVDF membranes were blocked with 5% skim milk powder and washed with PBST (PBS containing 0.1% Tween-20). After blocking, the membranes were washed with PBST and incubated overnight at 4°C with primary antibodies: mouse anti-Myc-Tag monoclonal antibody (9B11, Cell Signaling Technology) to detect the anti-PD-L1 scFv protein, and rabbit anti-β-actin monoclonal antibody (13E5, Cell Signaling Technology) as a loading control. Following three washes with TBST (Tris-buffered saline with 0.1% Tween-20), the membranes were incubated with HRP-conjugated secondary antibodies for 1 hour at room temperature. After additional washes with TBST, the protein bands were visualized using the ECL Prime chemiluminescent reagent (GE Healthcare). "

We sincerely appreciate your attention to this detail and thank you for helping us improve the quality of our manuscript.

Q: *7. Figure 3l requires a negative control to demonstrate that nanovesicles can still induce IFN-β secretion from dendritic cells. Furthermore, the authors stated in lines 202-203 that their nanovesicles maintained the activity of the STING agonists, yet no evidence has been presented in their results to support STING activation. I recommend the authors to perform a Western Blot or another experiment to directly validate their conclusion.*

R: Thank you for your valuable suggestions. Per your suggestion, we have included dendritic cells (DCs) treated with PBS and aPD-L1 NVs (nanovesicles without cGAMP) as negative control groups in our experiments. This addition reflects the basal secretion level of IFN-β from DCs and confirms that the induction of IFN-β is specifically due to the cGAMP-loaded nanovesicles.

STING (Stimulator of Interferon Genes) is a key protein in innate immune responses. When activated, STING triggers a signaling cascade leading to the phosphorylation and nuclear translocation of IRF3. This process results in the transcription of type I interferons (IFN-α and IFN-β) and interferon-stimulated genes (ISGs). Researchers typically evaluate STING activation by detecting cytokine secretion levels (type I interferons like IFN-β) via ELISA, the expression levels of phosphorylated IRF3 or TBK1 proteins using Western blot, or the mRNA levels of ISGs (such as *IFNB1, IFIT1, IFIT2, and ISG15*) through qPCR[7, 8, 9].

In our original manuscript, we co-incubated dendritic cells with aPD-L1 NVs@cGAMP stored for different durations and assessed whether aPD-L1 NVs@cGAMP maintained its STING agonist activity by measuring changes in IFN-β secretion levels. While this method provides evidence of STING activation, we acknowledge that additional data would further strengthen our conclusions.

Therefore, following your suggestion, we conducted additional experiments using quantitative PCR (qPCR) to detect changes in the mRNA levels of key interferon-stimulated genes. Specifically, after co-incubating dendritic cells with aPD-L1 NVs@cGAMP stored for different durations for 12 hours, we collected and measured the mRNA expression levels of *IFNB1, IFIT1, IFIT2, and ISG15*. The

results indicate that both stored and freshly prepared (Day 0) aPD-L1 NVs@cGAMP induce similar levels of these mRNAs in DCs, demonstrating that the nanovesicles maintain their STING agonist activity over time.

We have incorporated these new results into **Supplementary Figure 11** of the revised manuscript and have added corresponding discussions. The new data are as follows:

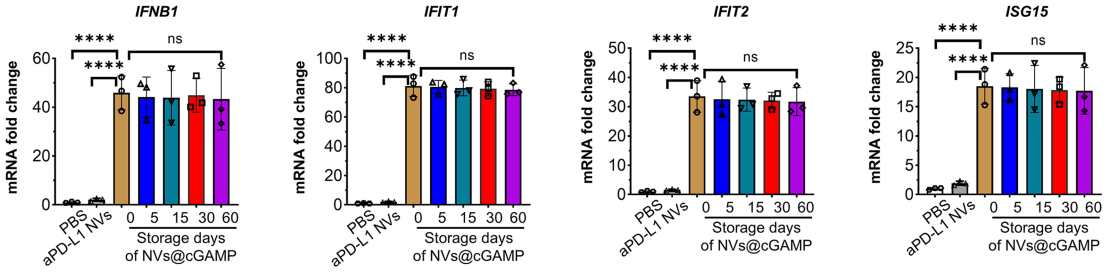

Supplementary Figure 11. After storage of aPD-L1 NVs@cGAMP at -80°C for varying durations, co-culture with dendritic cells (DCs) resulted in altered mRNA expression levels of *IFNB1*, *IFIT1, IFIT2, and ISG15* in DCs. DCs treated with PBS and aPD-L1 NVs served as negative controls (n = 3). All data are expressed as mean ± S.D. ****$p \leq 0.0001$ by one-way ANOVA with Tukey's post-test.

Q: *8. In figure 4a, it would be valuable for the authors to provide an explanation as to why the co-administration of NVs@cGAMP and aPD-L1 NVs did not result in a significant increase in the IFN-β concentration. Additionally, the claim made by the authors regarding the co-administration of aPD-L1 NVs and free STING agonists not significantly increasing the IFN-β concentration in the supernatant (as mentioned in lines 217-218) should be aligned with the corresponding data in figure 4a. Furthermore, it would be of interest to elucidate the levels of other cytokines such as IFN-γ, IL-2, and TNF-α, to provide a more comprehensive understanding of the immune response elicited by the administered treatments. Clarifying these aspects will contribute to a more thorough interpretation of the results.*

R: Thank you for pointing out the issues related to Figure 4a. We sincerely apologize for any confusion caused by our oversight. In the original manuscript, we mistakenly labeled the group "cGAMP + aPD-L1 NVs" (co-administration of aPD-L1 nanovesicles and free STING agonist cGAMP) as "NVs@cGAMP + aPD-L1 NVs" in Figures 4a, 4c, and 4e. This error led to inconsistencies between the data presented in Figure 4a and the descriptions in the manuscript. In the revised manuscript, this has been corrected to "cGAMP + aPD-L1 NVs". Therefore, our original intention was to convey that co-administration of cGAMP and aPD-L1 NVs does not result in a significant increase in IFN-β levels.

NVs@cGAMP demonstrates superior efficacy in promoting the release of inflammatory cytokines compared to the cGAMP + aPD-L1 NVs group. This enhancement is likely due to improved cellular uptake and retention of the STING agonist when encapsulated within nanovesicles. Generally, STING agonists are

hydrophilic and negatively charged, which limits their ability to penetrate cell membranes and results in poor cellular uptake. Additionally, free STING agonists are prone to degradation by phosphodiesterases in circulation and on the cell surface, leading to a shorter half-life[4, 5, 6, 7]. In contrast, nanovesicles, with their lipid bilayer structure, can facilitate rapid cellular entry, thereby improving the intracellular delivery and retention of STING agonists. This phenomenon has been previously demonstrated in studies such as that by Kathleen M et al., where STING agonist-loaded extracellular vesicles exhibited a tenfold increase in cellular uptake compared to free STING agonists[8, 9]. We have included this explanation in the revised manuscript to clarify the enhanced efficacy of NVs@cGAMP, as follows:

TNF-α secretion enhancement. This synergistic effect may be attributed to aPD-L1 NVs facilitating the cellular uptake of STING agonists. Typically, STING agonists are hydrophilic and negatively charged, which limits their ability to penetrate cell membranes and results in poor cellular uptake[48, 49]. Moreover, free STING agonists are readily degraded by phosphodiesterases on the cell surface and in circulation, leading to a short half-life[50]. In contrast, nanovesicles with lipid bilayer structures can facilitate rapid entry into cells via endocytosis or membrane fusion, thereby improving the intracellular delivery and retention of STING agonists[51]. Studies by Kathleen M. et al. have demonstrated that loading STING agonists into extracellular vesicles increased cellular uptake tenfold compared to free STING agonists[49].

Additionally, following your valuable suggestion, we have measured the levels of additional cytokines, including IFN-γ, IL-2, and TNF-α. The results indicate that NVs@cGAMP effectively promotes the secretion of these cytokines, which are critical mediators of antitumor immune responses. We have incorporated these new results into **Supplementary Figure 12** of the revised manuscript.

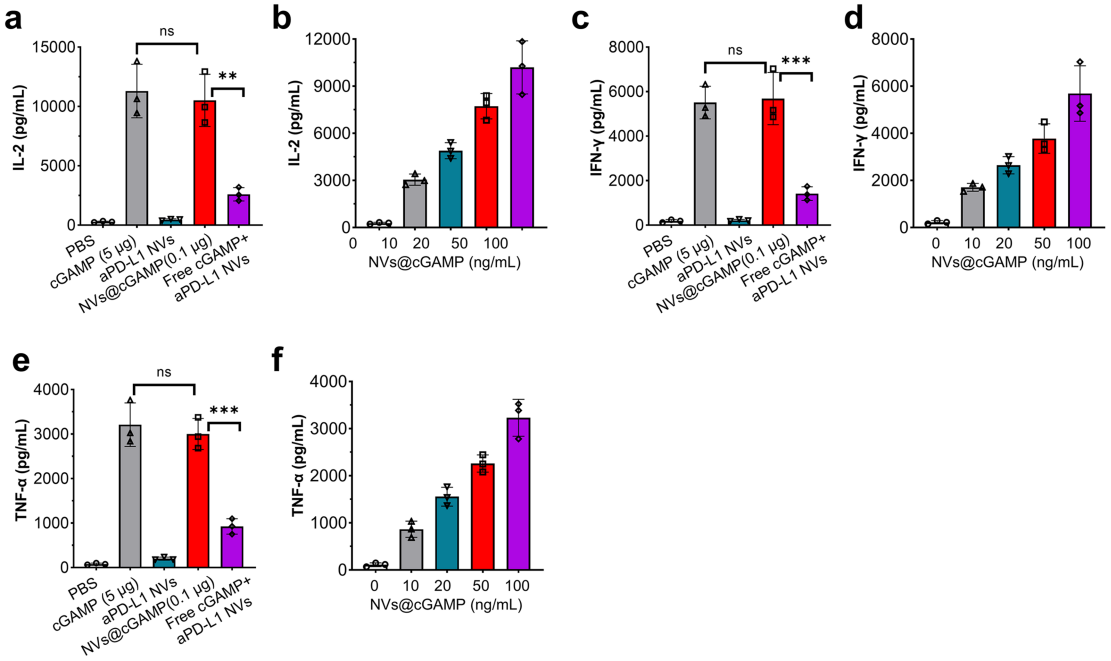

Supplementary Figure 12. (a, c and e) IL-2, IFN-γ and TNF-α levels in the supernatants after 12 h of addition of different agents to the co-incubation system of CAR-T cells, DCs and LLC-MSLN cells were assessed by ELISA (n = 3). (b, d and f) After adding different doses of aPD-L1 NVs@cGAM to the co-incubation system of CAR-T cells, DCs and LLC-MSLN cells for 12 h, the dose-dependent release of IL-2, IFN-γ and TNF-α was detected by ELISA (n = 3). ns: not significant, $^{**}p \leq 0.01$, $^{***}p \leq 0.001$ by one-way ANOVA with Tukey's post-test for (a), (c) and (e).

Q: *9. In figure 4c-f, the description concerning how the experiments were conducted remains unclear. In addition, the authors need to explain the rationale behind the inclusion of DCs in the co-culture system. They also need to provide detailed experimental procedures in the methods section.*

R: Thank you for your insightful comments. In this study, we included dendritic cells (DCs) in the co-culture system to better simulate the in vivo tumor microenvironment and to elucidate the interactions between NVs@cGAMP, DCs, and CAR-T cells. DCs play a pivotal role in modulating immune responses within tumors. In the tumor microenvironment, DCs typically exhibit high expression of PD-L1, which is further upregulated upon activation by STING agonists[21, 22, 23]. Therefore, NVs@cGAMP with PD-L1 targeting preferentially target both DCs and tumor cells. Upon uptake by DCs, NVs@cGAMP activates the STING pathway, leading to DC maturation. Mature DCs secrete elevated levels of pro-inflammatory cytokines (e.g., IFN-β and IL-12) and express high levels of co-stimulatory molecules (e.g., CD80, CD86). These pro-inflammatory cytokines and co-stimulatory signals significantly enhance the proliferation and anti-tumor cytotoxicity of CAR-T cells by providing essential activation and survival cues. Therefore, including DCs in the co-culture system allows us to more accurately assess the immunomodulatory effects of NVs@cGAMP on CAR-T cell function.

We have added the rationale for including DCs in the co-culture system to the revised manuscript, as follows:

CAR-T cells. Crucially, since dendritic cells (DCs) within the tumor microenvironment often overexpress PD-L1 and are primary target cells for STING agonists[46, 47], we included DCs in the experiment to more accurately simulate how aPD-L1 NVs@cGAMP enhances the antitumor capacity of CAR-T cells *in vivo*.

Additionally, in accordance with your suggestion, we have provided detailed experimental procedures related to Figures 4c–f in the Methods section of the revised manuscript, as detailed below:

Assessment of NVs@cGAMP on MSLN CAR-T cell cytotoxicity and proliferation

The effect of NVs@cGAMP on the cytotoxicity of MSLN CAR-T cells was evaluated as previously described[77, 78, 79]. Briefly, 2×10^4 luciferase-expressing LLC-MSLN cells, 1×10^4 CAR-T cells, and 2×10^3 dendritic cells were seeded into white opaque 96-well plates. Different treatments were added as required, and the cells were incubated at 37 °C with 5% CO_2 for 12 hours. Wells containing LLC-MSLN cells alone (without effector cells) served as positive controls to determine maximum luciferase activity. After co-incubation, the supernatant was gently removed, and cell lysis buffer (Promega) was added according to the manufacturer's instructions, followed by the addition of 10 µL Steady-Glo luciferase substrate (Promega). After a 5-minute incubation, luminescence was measured using an EnVision multimode plate reader (PerkinElmer). The cytotoxicity of CAR-T cells was calculated based on the luminescence readings using the following formula: % Killing = 100− [(RLU from co-culture wells/RLU from control wells) × 100]

For proliferation assessment, LLC-MSLN cells, GFP-expressing CAR-T cells, and dendritic cells were seeded into 12-well plates at a ratio of 10:5:1. Different treatments were added as required, and the cells were incubated at 37 °C with 5% CO_2 for 5 days. During this period, the culture medium was refreshed as necessary based on the proliferation rate of CAR-T cells to ensure adequate nutrient supply. After 5 days, cells were harvested and counted using flow cytometry.

Q: *10. The authors should provide an explanation on why both aPD-L1 NVs@cGAMP and free STING agonist treatments led to a significant upregulation of PD-L1 mRNA levels in tumor tissues (as depicted in figure 5d), while also enhancing the cytotoxicity of CAR-T cells (illustrated in figure 4e-f).*

R: Thank you for pointing out this important issue. We acknowledge that both aPD-L1 NVs@cGAMP and free STING agonist treatments led to a significant upregulation of PD-L1 mRNA levels in tumor tissues (Figure 5d), which could potentially inhibit CAR-T cell function due to increased PD-L1 expression. However, we observed an enhancement in the cytotoxicity of CAR-T cells under these treatments (Figure 4e-f).

We propose several possible explanations for this observation:

(1) STING agonists activate the production of type I interferons and pro-inflammatory cytokines (e.g., IL-2, IL-15, IL-18), which may enhance T cell activation and proliferation, potentially offsetting the inhibitory effects of increased PD-L1 expression[24, 25].

(2) Activation of STING enhances the maturation of dendritic cells (DCs). Mature DCs can augment CAR-T cell function through direct cell-to-cell contact or by secreting supportive cytokines[22, 26].

(3) STING pathway activation might induce a stem-cell-like phenotype in $CD8^+$ T cells, enhancing their longevity and function even in the presence of inhibitory signals like PD-L1[4, 5].

(4) STING agonists may sensitize tumor cells to T cell-mediated killing by inducing stress and apoptosis pathways[6, 27].

(5) STING activation may increase chemokine expression, facilitating CAR-T cell infiltration into tumor tissues. Additionally, upregulation of MHC class I molecules on tumor cells might improve recognition by CAR-T cells[5, 7, 27].

Therefore, although STING agonists can potentially impair CAR-T cell function by upregulating PD-L1 expression, the overall effect is an enhancement of CAR-T cell antitumor activity due to these additional mechanisms. In our study, the use of aPD-L1 NVs@cGAMP effectively blocks most of the elevated PD-L1, further enhancing the antitumor efficacy of CAR-T cells.

We have incorporated this explanation into the revised manuscript. Thank you for your valuable feedback.

Q: *11. In lines 305-307, the authors asserted that aPD-L1 NVs@cGAMP demonstrate the ability to reverse immunosuppressive tumor microenvironments and inhibit metastatic growth in vivo. The authors should consider utilizing flow cytometry to assess specific immune cell populations, specifically targeting T cell subsets (including Th1, Th2, Th17, effector T cells, memory T cells, etc.), MDSCs, and other relevant markers associated with T cell exhaustion such as TIM3, LAG3, and*

TIGIT. This approach would facilitate the identification of any alterations within the immunosuppressive tumor microenvironment, offering valuable insights into the effects of the treatment.

R: Thank you for your insightful comments. We fully agree that additional evidence is necessary to substantiate our assertion about the capabilities of aPD-L1 NVs@cGAMP. Per your suggestion, we have performed comprehensive flow cytometry analyses to evaluate specific immune cell populations within the tumor microenvironment, including T cell subsets, T cell exhaustion markers, and myeloid-derived suppressor cells (MDSCs).

Our findings indicate that treatment with aPD-L1 NVs@cGAMP significantly increased the proportions of Th1 and Th17 cells, which are associated with pro-inflammatory and anti-tumor immune responses (**Fig. 5g and Fig. 5i**). Concurrently, there was a notable reduction in Th2 cells and MDSCs, both of which contribute to immunosuppression within the tumor microenvironment (**Fig. 5d and Fig. 5g**). Furthermore, although T cell exhaustion markers (PD-1, TIM3, LAG3, and TIGIT) remain elevated in the aPD-L1 NVs@cGAMP treatment group, their expression levels are significantly lower than those observed in the group treated with free cGAMP alone (**Fig. 5e)**. This indicates a partial reversal of T cell exhaustion, which is crucial for restoring T cell functionality against tumor cells. Importantly, we observed a marked increase in both effector memory T cells and central memory T cells in the aPD-L1 NVs@cGAMP group compared to other treatment groups (**Fig. 5h and Fig. 5j**). The expansion of these memory T cell populations is crucial for maintaining long-term anti-tumor immunity and reducing the likelihood of tumor recurrence.

We have incorporated these new findings and the corresponding discussion into the revised manuscript. The updated figure is as follows:

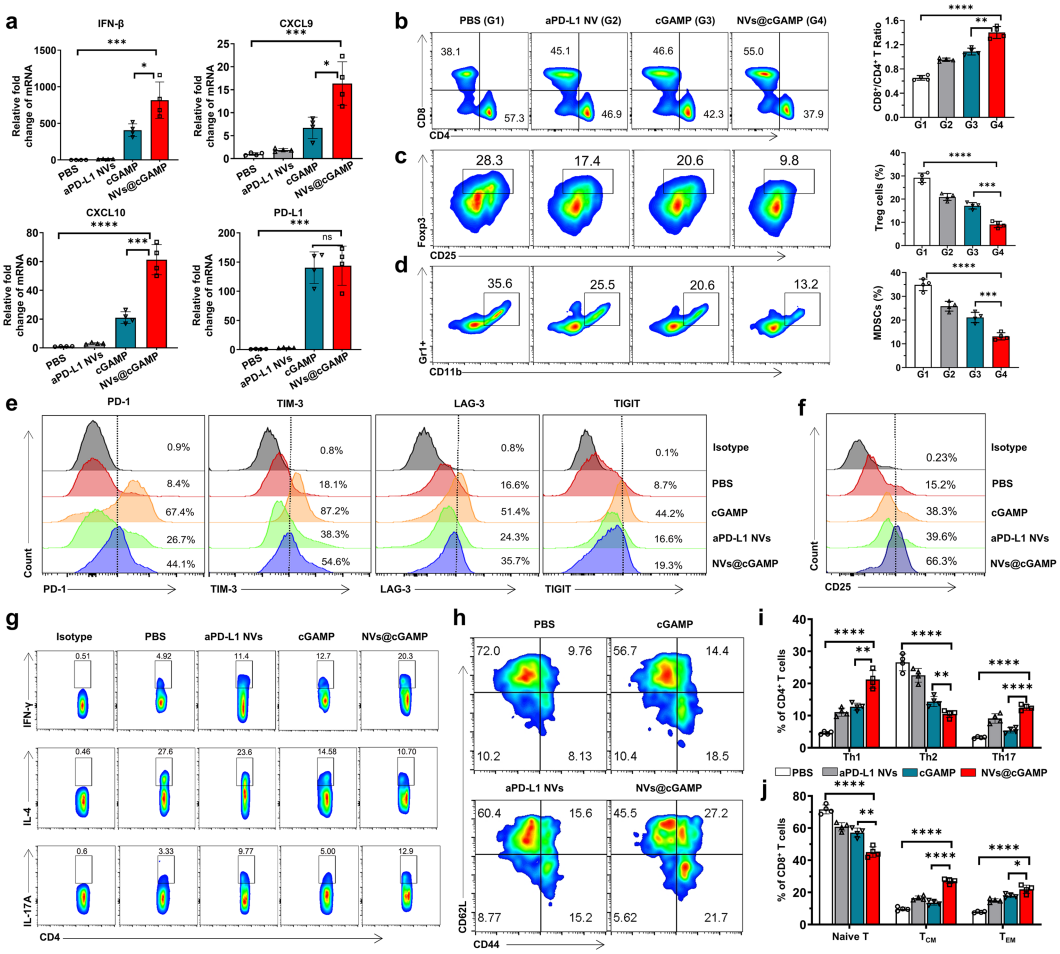

Figure 5. Remodeling of the tumor microenvironment and inhibition of tumor growth by aPD-L1 NVs@cGAMP. (b-d) Representative flow cytometry plots and statistical analysis of (b) $CD8^+$ T cells and $CD4^+$ T cells, (c) Treg cells and (d) MDSCs within the TME across various treatment groups (n = 4). (e) Analysis of T cell exhaustion markers PD-1, TIM-3, LAG-3, and TIGIT in different treatment groups by flow cytometry. (f) Expression levels of CD25 on T cells in different treatment groups, analyzed by flow cytometry. (g, i) Representative flow cytometry plots and statistical analysis of Th1, Th2, and Th17 cells within the TME across different treatment groups (n = 4). (h, j) Representative flow cytometry plots and statistical analysis of naïve T cells, central memory T cells (T_{CM}), and effector memory T cells (T_{EM}) within the TME across different treatment groups (n = 4).

Q: *12. In figure 6b, I recommend using nanovesicles without cGAMP as a control, as PBS alone is not sufficiently rigorous for this comparison. This adjustment is necessary because it ensures a more accurate evaluation of the specific impact attributed to the inclusion of cGAMP in the nanovesicles.*

R: Thank you for your insightful suggestion. We completely agree that using nanovesicles without cGAMP (aPD-L1 NVs) as a control provides a more rigorous comparison than using PBS alone. In fact, we have presented the therapeutic effect of aPD-L1 NVs in **Figure 5m** of the original manuscript. However, as you rightly

pointed out, including the aPD-L1 NVs group as a control in **Figure 6b** will more clearly evaluate the specific impact of incorporating cGAMP into the nanovesicles.

Accordingly, we have updated **Figure 6b** in the revised manuscript to include the aPD-L1 NVs group as a control in both the LLC and B16 tumor models. The updated figure is as follows:

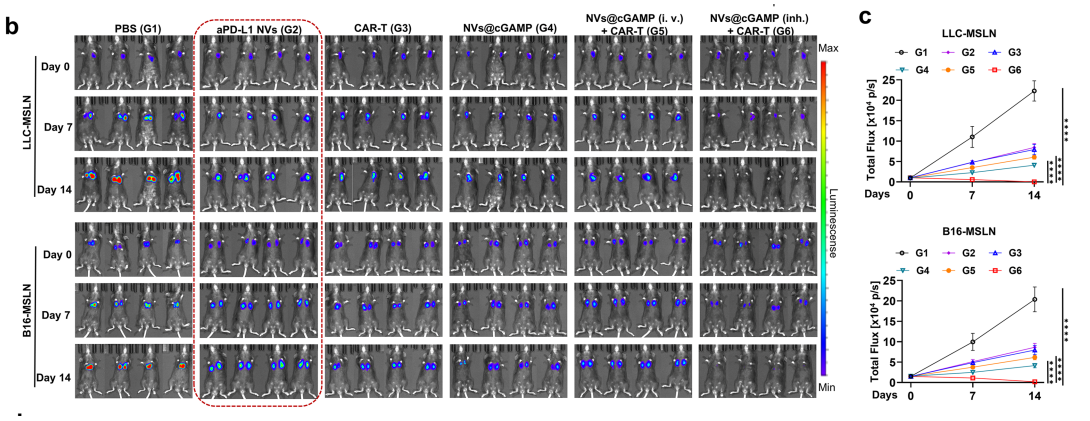

Figure 6. (b-c) Bioluminescence was measured by the IVIS system to evaluate tumor growth in the different treatment groups, and the bioluminescence intensity was statistically analyzed (n = 4).

We sincerely appreciate your valuable feedback, which has helped us improve the rigor and clarity of our study.

Q: *13. For all in vivo experiments in this study, the authors need to monitor and present the percentages of CAR-T cells at different time points. This practice ensures a comprehensive understanding of the persistence and behavior of CAR-T cells within the experimental model across the duration of the study.*

R: Thank you for your insightful suggestion. In accordance with your recommendation, we have monitored and presented the percentages of CAR-T cells at different time points in all our in vivo experiments involving CAR-T cells. Specifically, we collected peripheral blood samples from mice via tail vein at designated intervals and assessed CAR-T cell expansion using flow cytometry. These additional studies demonstrate that NVs@cGAMP effectively enhances the in vivo expansion and persistence of CAR-T cells, which is crucial for improving the efficacy of tumor immunotherapy. We have incorporated these results into **Supplementary Fig. 7, Supplementary Fig. 19** and **Supplementary Fig. 29-30** of the revised manuscript and have updated the discussion to reflect these findings. The newly added figures are provided below:

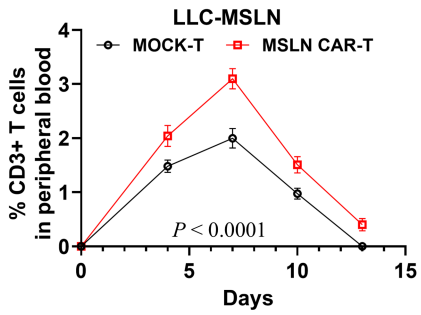

Supplementary Fig. 7. Following injection of GFP-expressing MOCK-T or MSLN CAR-T cells into LLC-MSLN tumor-bearing mice, flow cytometry was used to analyze the percentage of CAR-T cells in peripheral blood at various time points (n = 4). ****$p \leq 0.0001$ by two-way ANOVA with Tukey's post-test.

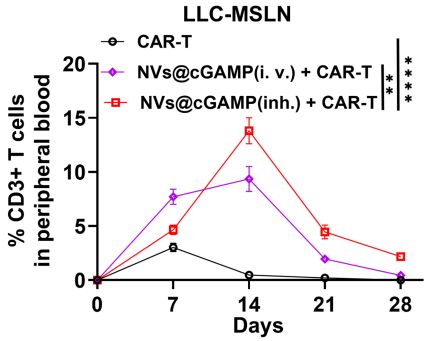

Supplementary Figure 19. The percentage of CAR-T cells in the peripheral blood of LLC-MSLN tumor-bearing mice was analyzed by flow cytometry at various time points following different treatments. Data are expressed as mean ± S.D. **$p \leq 0.01$, ****$p \leq 0.0001$ by two-way ANOVA with Tukey's post-test.

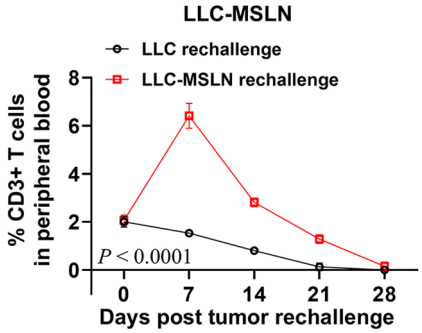

Supplementary Figure 29. After cured mice were rechallenged with either mesothelin (MSLN)-overexpressing tumor cells or parental cells, the percentage of CAR-T cells in the peripheral blood of LLC-MSLN tumor-bearing mice was analyzed by flow cytometry at different time points. Data are presented as the mean ± S.D. ****$p \leq 0.0001$ by two-way ANOVA with Tukey's post-test.

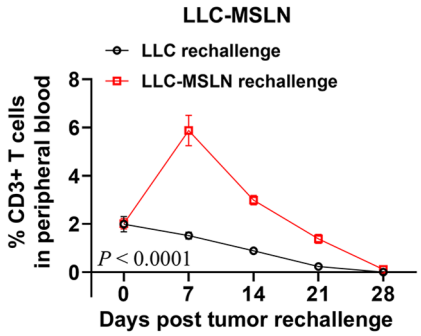

Supplementary Figure 30. Following subcutaneous injection of MSLN-overexpressing tumor cells or parental cells into the inguinal region of cured mice, the percentages of CAR-T cells in the peripheral blood of LLC-MSLN tumor-bearing mice were analyzed over time. Data are presented as the mean ± S.D. ****$p \leq 0.0001$ by two-way ANOVA with Tukey's post-test.

Q: *14. In figures 6c, e, f, and g, it is recommended that the authors annotate the differences between the data and specify the statistical analysis methods used in the figure legends. This practice will enhance the comprehensibility of the experimental results and bolster their credibility.*

R: Thank you for your valuable suggestion. Per your suggestion, we have updated the figures you mentioned, as well as other relevant figures, to include annotations of the statistical differences between the groups. Additionally, we have specified the statistical analysis methods used in each figure legend.

Q: *15. In figure 7, the sole detection of M1 macrophages is insufficient to support a conclusion that the tumor microenvironment was changed. Additionally, it is advisable to charaterize M2 macrophages and other T cell subsets, and measure the levels of cytokines such as interleukin-10 and TGF-β. This approach will provide a more comprehensive evaluation of the immune landscape within the tumor microenvironment.*

R: Thank you for your insightful comments. We agree that detecting only M1 macrophages is insufficient to conclusively demonstrate changes in the tumor microenvironment.

Per your suggestion, we have conducted additional experiments using flow cytometry to assess changes in macrophage polarization (M1 and M2) and various T cell subsets ($CD8^+$ T cells, Th1, Th2, Th17), within the TME. Our results demonstrate that treatment with aPD-L1 NVs@cGAMP significantly increased the proportions of M1 macrophages, $CD8^+$ T cells, Th1 cells, and Th17 cells, while decreasing the proportions of M2 macrophages and Th2 cells. This shift indicates a reprogramming of the immune milieu from an immunosuppressive to an immunostimulatory state, which is conducive to enhancing anti-tumor immunity.

Furthermore, we measured the levels of anti-inflammatory cytokines interleukin-10 (IL-10) and transforming growth factor-beta (TGF-β) in the TME using ELISA assays. The results showed that the secretion levels of IL-10 and TGF-β in the aPD-

L1 NVs@cGAMP treatment group were significantly lower than those in other treatment groups. The reduction of these cytokines, which are known to contribute to tumor progression and immune evasion, further supports the effectiveness of our treatment in modulating the TME.

We have incorporated these updated results and the corresponding discussion into the revised manuscript. The updated figure is as follows:

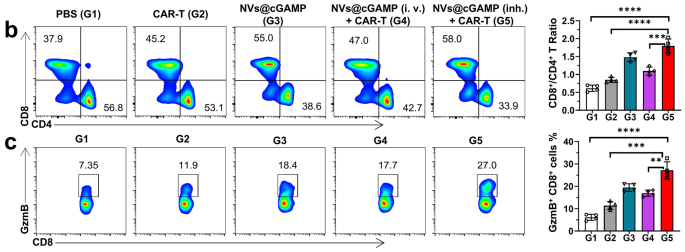

Figure 7. (b-c) Representative flow cytometry plots and statistical analysis of (b) $CD8^+$ T cells and $CD4^+$ T cells and (c) infiltrating granzyme B-expressing $CD8^+$ T cells within the TME across various treatment groups (n = 4).

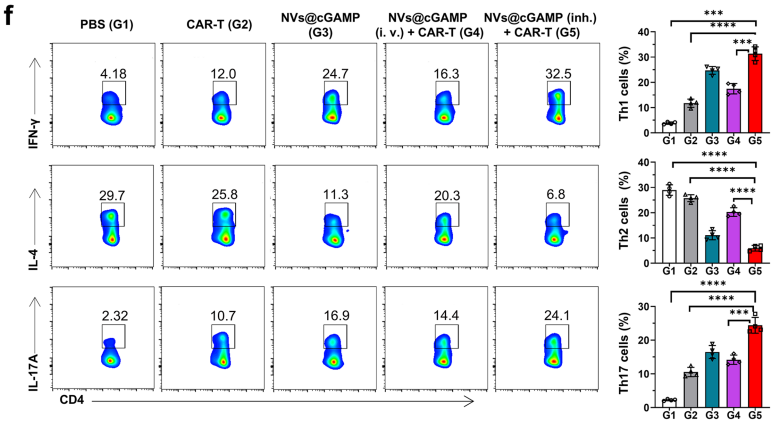

Figure 7. (f) Representative flow cytometry plots and statistical analysis of Th1, Th2 and Th17 within the TME across various treatment groups (n = 4).

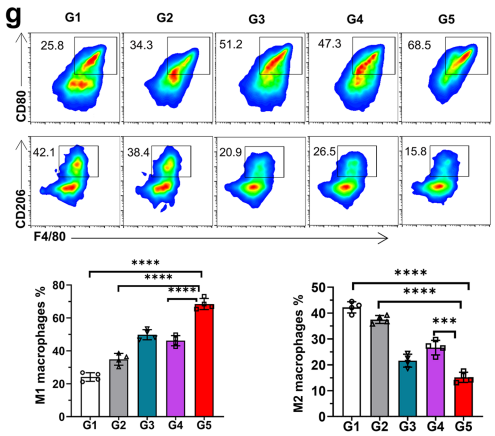

Figure 7. (g) Representative flow cytometry plots and statistical analysis of M1-type and M2-type

macrophages within the TME across various treatment groups (n = 4).

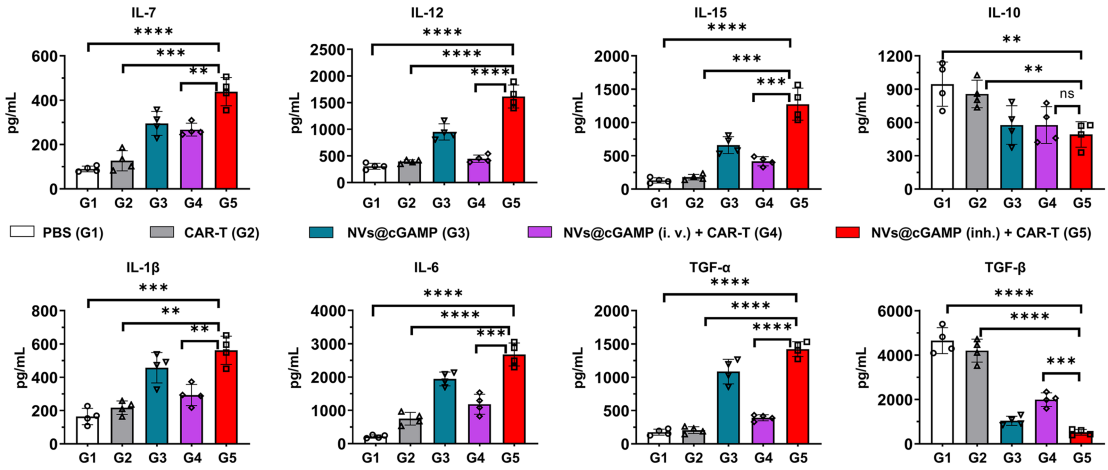

Supplementary Figure 26. Cytokine concentrations of IL-7, IL-12, IL-15, IL-10, IL-1β, IL-6, TGF-α and TGF-β in tumor tissue homogenates from different treatment groups were quantified by ELISA (n = 4). Data are presented as the mean ± S.D. $^{**}p \leq 0.01$, $^{***}p \leq 0.001$, $^{****}p \leq 0.0001$ by one-way ANOVA with Tukey's post-test.

Q: *16. In lines 379-381, the author concluded that mature DCs activate CAR-T cells and support the development of long-term antitumor immune memory by presenting tumor antigens to T cells. However, there is a lack of correlated results to substantiate that the upregulation of CD80 and CD86 in DCs effectively activates CAR-T cells and promotes their long-term antitumor effect. Providing additional correlated data would strengthen the claim regarding the functional impact of mature DCs on CAR-T cell activation and long-term antitumor responses.*

R: Thank you for your insightful comment. We fully agree that additional evidence is necessary to substantiate the impact of mature dendritic cells (DCs) on CAR-T cell activation and their long-term antitumor efficacy.

In our study, we demonstrated that NVs@cGAMP effectively promotes DC maturation. It is well-established that mature DCs upregulate costimulatory molecules such as CD80 and CD86 and secrete pro-inflammatory cytokines, which are critical for T cell activation. Specifically, CD80 and CD86 interact with the CD28 receptor on T cells, providing essential co-stimulatory signals for full T cell activation and proliferation.

To specifically evaluate the effect of upregulated CD80 and CD86 on DCs in activating CAR-T cells and enhancing their long-term antitumor function, we conducted *in vivo* blocking experiments. We established the LLC tumor model as previously described and treated tumor-bearing mice with either CAR-T cells alone or a combined therapy of CAR-T cells with NVs@cGAMP. In the intervention group, mice receiving the combined therapy were injected every three days with anti-CD80 and anti-CD86 blocking antibodies (10 mg/kg) to inhibit CD80 and CD86 function on the surface of DCs until the end of the treatment.

On day 14 post-treatment, we analyzed the effect of blocking CD80 and CD86 on DCs on CAR-T cell activation and memory cell phenotypes using flow cytometry. The results showed that, compared to the combined therapy group without antibody blocking, the group receiving both anti-CD80 and anti-CD86 antibodies exhibited a significant decrease in CD69 expression on CAR-T cells, indicating that antibody blocking impaired CAR-T cell activation. Additionally, the proportions of central memory CAR-T cells (T_{CM}) and effector memory T cells (T_{EM}) were significantly reduced in the antibody-blocked group, suggesting that blocking CD80 and CD86 adversely affected the development of CAR-T cell memory and their long-term antitumor capacity.

These findings highlight the critical role of mature DCs in enhancing CAR-T cell activation and sustaining their antitumor activity. While NVs@cGAMP can directly stimulate CAR-T cells through STING pathway activation, the maturation of DCs and subsequent costimulatory interactions significantly augment this effect.

We have incorporated these new findings and the corresponding discussion into the revised manuscript. The updated figure is as follows:

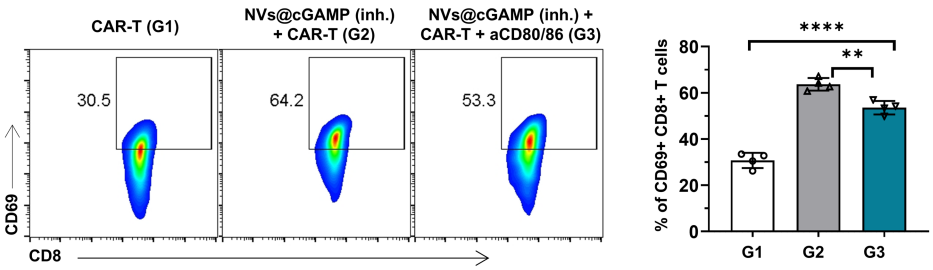

Supplementary Figure 25. Representative flow cytometry plots and statistical analysis of CD69 expression on CAR-T cells in peripheral blood across various treatment groups ($n = 4$). Data are presented as the mean ± S.D. $^{**}p \leq 0.001$, $^{****}p \leq 0.0001$ by one-way ANOVA with Tukey's post-test.

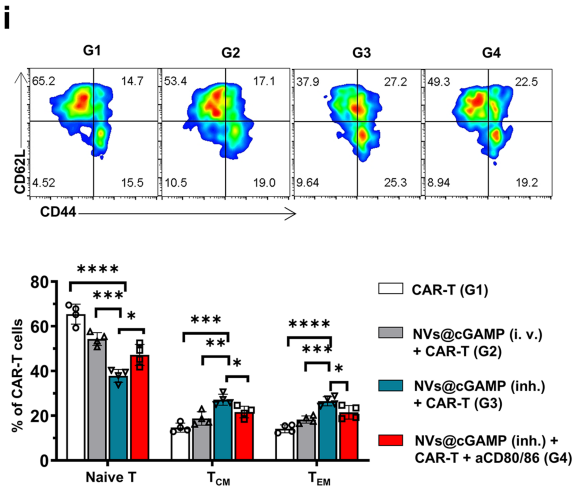

Figure 7. (i) Representative flow cytometry plots and statistical analysis of naïve T cells, central memory T cells (T_{CM}), and effector memory T cells (T_{EM}) within the CAR-T cell population in the TME across different treatment groups ($n = 4$).

Q: *17. In lines 398-400, the author inferred that aPD-L1 NVs@cGAMP effectively reversed the immunosuppressive tumor microenvironment, rendering it proinflammatory and conducive to CAR-T cell proliferation and function. However, the evidences provided are not sufficient to support these conclusions. To substantiate the claim that the tumor microenvironment becomes proinflammatory, the authors should measure the levels of proinflammatory cytokines such as TNF-α, IL-6, and IL-1β within the tumor microenvironment. Furthermore, evaluating the presence and activation state of proinflammatory immune cells such as Th1 cells, cytotoxic T cells, and assessing the expression of inducible nitric oxide synthase (iNOS) and cyclooxygenase-2 (COX-2) would strengthen their case. Additionally, to demonstrate that CAR-T cell proliferation was enhanced, the percentage of CAR-T cells should be quantified. Incorporating these approaches will provide more robust evidence for the conclusions drawn.*

R: Thank you for your valuable suggestions. We fully agree that more robust evidence is necessary to substantiate our conclusion.

Following your recommendations, we first measured the levels of proinflammatory cytokines (TNF-α, IL-6, and IL-1β) within the tumor microenvironment to confirm its proinflammatory shift. Our ELISA results demonstrated that the secretion levels of TNF-α, IL-6, and IL-1β in the group treated with inhaled aPD-L1 NVs@cGAMP combined with CAR-T cells were significantly higher than those in the PBS and CAR-T cell-only treatment groups (**Supplementary Figure 26**). This indicates that the tumor microenvironment transitioned from an anti-inflammatory to a proinflammatory state to some extent.

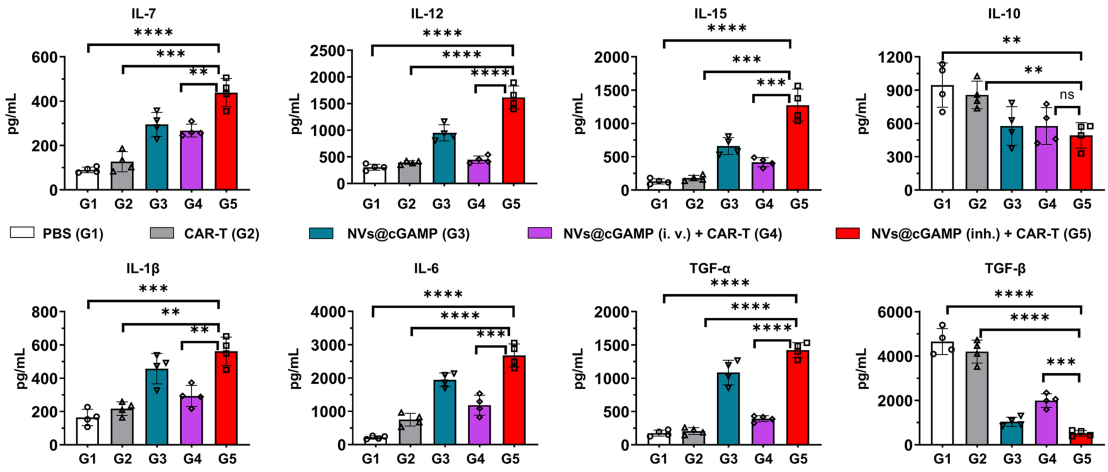

Supplementary Figure 26. Cytokine concentrations of IL-7, IL-12, IL-15, IL-10, IL-1β, IL-6, TGF-α and TGF-β in tumor tissue homogenates from different treatment groups were quantified by ELISA (n = 4). Data are presented as the mean ± S.D. $^{**}p \leq 0.01$, $^{***}p \leq 0.001$, $^{****}p \leq 0.0001$ by one-way ANOVA with Tukey's post-test.

Next, we evaluated the proportions and activation states of Th1 cells and cytotoxic T cells using flow cytometry. The results showed that, compared to other treatment groups, the combination of inhaled aPD-L1 NVs@cGAMP and CAR-T cells

significantly increased the proportions of Th1 and $CD8^+$ T cells within the tumor microenvironment (**Fig. 7b and Fig. 7f**). Importantly, $CD8^+$ T cells in this group expressed higher levels of CD69 and granzyme B compared to other groups (**Fig. 7c and Supplementary Fig. 23**). CD69 is an early activation marker, while granzyme B is a critical enzyme that mediates the cytotoxic activity of T cells. The elevated expression of these markers indicates that inhaled aPD-L1 NVs@cGAMP effectively activates endogenous T cells.

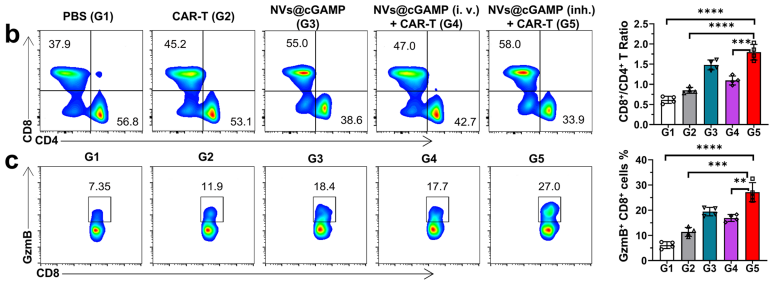

Figure 7. (b-c) Representative flow cytometry plots and statistical analysis of (b) $CD8^+$ T cells and $CD4^+$ T cells and (c) infiltrating granzyme B-expressing $CD8^+$ T cells within the TME across various treatment groups (n = 4).

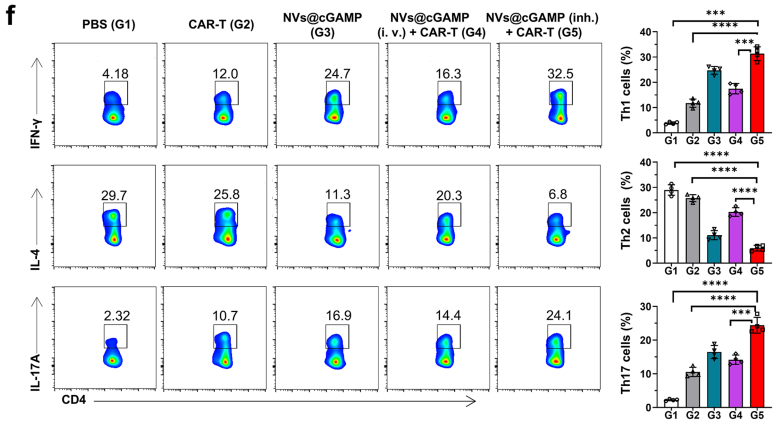

Figure 7. (f) Representative flow cytometry plots and statistical analysis of Th1, Th2 and Th17 within the TME across various treatment groups (n = 4).

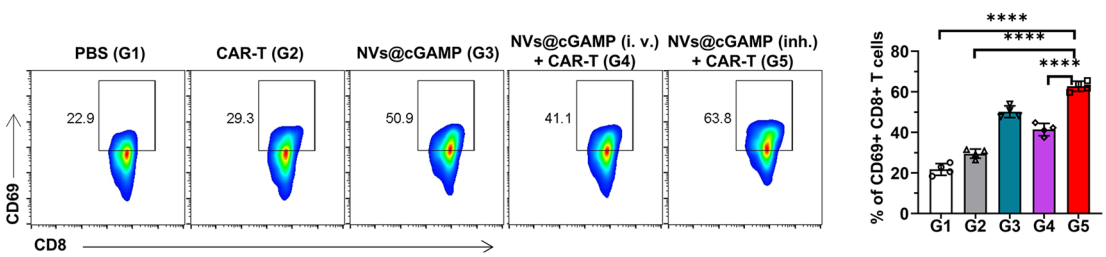

Supplementary Figure 23. Representative flow cytometry plots and statistical analysis of CD69 expression on T cells within the TME across various treatment groups (n = 4). Data are presented as the mean ± S.D. ****$p \leq 0.0001$ by one-way ANOVA with Tukey's post-test.

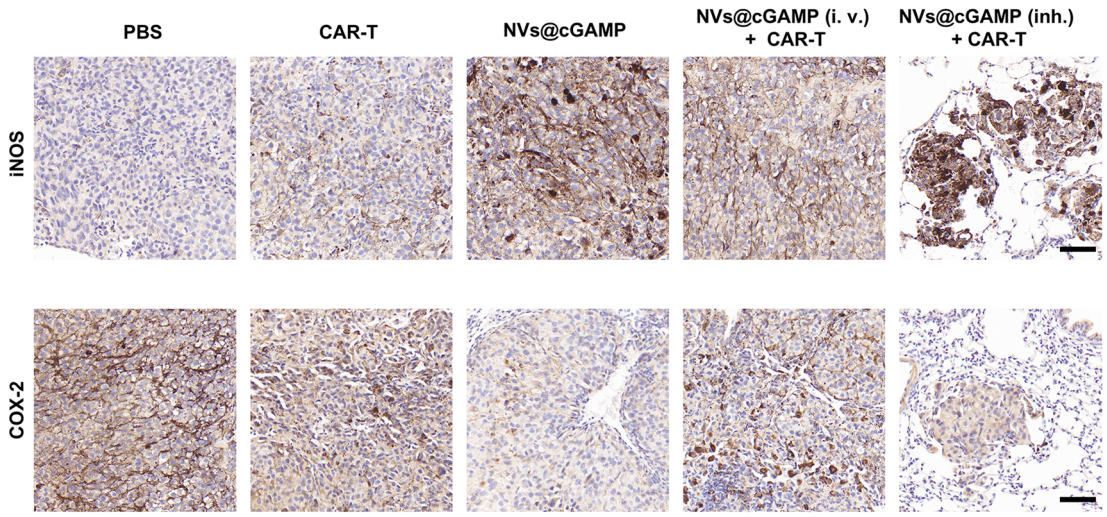

Supplementary Figure 24. Expression of iNOS and COX-2. (a-b) LLC-MSLN tumor-bearing mice receiving different treatments were assessed for (a) iNOS and (b) COX-2 expression in tumor tissues via immunohistochemistry. Scale bar: 200 μm.

Following your suggestion, we also assessed the expression levels of inducible nitric oxide synthase (iNOS) and cyclooxygenase-2 (COX-2) in lung tissue sections using immunohistochemistry. iNOS induces the production of nitric oxide (NO), and high levels of NO can cause DNA damage and apoptosis in tumor cells. Conversely, COX-2 plays a key role in prostaglandin synthesis, and elevated prostaglandins can promote angiogenesis and increase tumor cell invasiveness. The immunohistochemistry results showed that the combination therapy of CAR-T and NVs@cGAMP (inh.) effectively increased the expression of iNOS while reducing the expression of COX-2 (**Supplementary Figure 24)**.

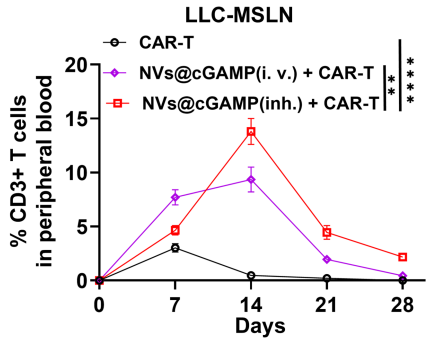

Supplementary Figure 19. The percentage of CAR-T cells in the peripheral blood of LLC-MSLN tumor-bearing mice was analyzed by flow cytometry at various time points following different treatments.

Finally, to comprehensively understand the proliferation and persistence of CAR-T cells, we quantified their percentages at different time points post-treatment using flow cytometry (**Supplementary Figure 19**).

We have incorporated the detailed methods, results, and significance of these experiments into the revised manuscript. Once again, thank you for your thorough and constructive suggestions.

Q: 18. *In lines 413-416, the authors conclude that the resistance to B16 cells in CAR-T+NVs@cGAMP-cured mice could be attributed to an enhanced epitope spreading phenomenon. However, the results provided are not sufficient to support this conclusion. I suggest the authors consider conducting additional experiments or provide further analyses to substantiate this proposed mechanism. This may involve evaluating adaptive immune responses against a broader range of tumor antigens or conducting assays focused on epitope spreading to validate the proposed rationale.*

R: Thank you for your insightful suggestion. We fully agree that additional experiments and analyses are necessary to substantiate whether the resistance to tumor cells lacking the target antigen in CAR-T + NVs@cGAMP-cured mice can be attributed to an enhanced epitope spreading phenomenon.

Epitope spreading is a phenomenon where the immune response extends beyond the initial target epitope to other epitopes on the same or different antigens. This typically occurs following the death of tumor cells induced by the initial immune response. The dying tumor cells release a variety of antigens that are captured by antigen-presenting cells (APCs) and presented to T cells, thereby initiating immune responses against these new antigens[28]. In the context of CAR-T cell therapy, activating endogenous $CD8^+$ T cells against antigens beyond the CAR-targeted antigen is critical for overcoming tumor heterogeneity and antigen-loss-mediated escape[29, 30].

To investigate whether CAR-T + NVs@cGAMP treatment can induce epitope spreading, we conducted additional experiments as per your recommendation. We engineered LLC-MSLN-OVA tumor cells by introducing ovalbumin (OVA) as a bystander antigen not targeted by our CAR-T cells. The OVA (257–264, SIINFEKL) peptide is a well-characterized model antigen presented by the mouse class I MHC molecule $H\text{-}2K^b$ and is commonly used to study $CD8^+$ T cell responses[30, 31]. Using the same methodology as before, we established an LLC-MSLN-OVA tumor-bearing mouse model and administered the identical treatment regimen. After 14 days, we isolated $CD8^+$ T cells from the mice's spleens for flow cytometric analysis. Compared to other treatment groups, mice receiving CAR-T + NVs@cGAMP treatment exhibited a significant increase in the frequency of OVA-specific (SIINFEKL-directed) $CD8^+$ T cells (**Fig. 8c-d and Supplementary Figure 27a-b**). Additionally, after ex vivo stimulation of the isolated splenic $CD8^+$ T cells with $OVA_{(257–264)}$ (SIINFEKL, 200 nM) for 4 hours, we observed a higher proportion of IFN-γ^+ $CD8^+$ T cells in the CAR-T + NVs@cGAMP treatment group. These results suggest that CAR-T + NVs@cGAMP treatment significantly enhances the host anti-tumor immune response and promotes epitope spreading to non-MSLN antigens.

We have incorporated the detailed methods, results, and significance of these experiments into the revised manuscript. Thank you once again for your constructive feedback, which has significantly improved our study. The updated findings are presented as follows:

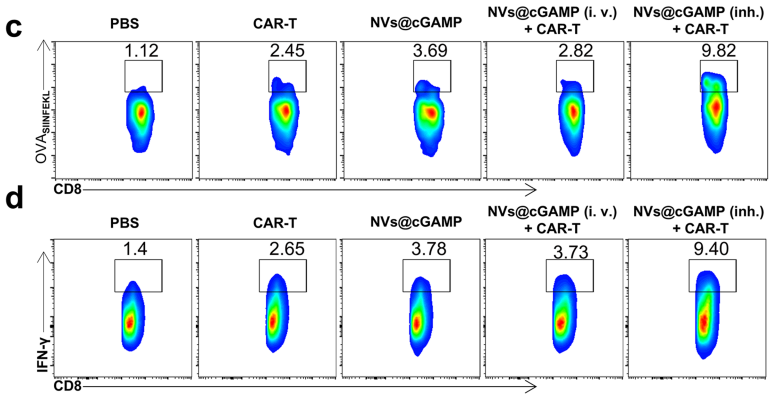

Figure 8. (c) In LLC-MSLN-OVA tumor-bearing mice, the percentage of OVA $_{(SIINFEKL)}$-specific $CD8^+$ T cells in the spleen was assessed via flow cytometry after various treatments. (d) Following stimulation with OVA peptides, the percentage of T cells producing IFN-γ within the $CD8^+$ T cell population in different treatment groups was evaluated by flow cytometry.

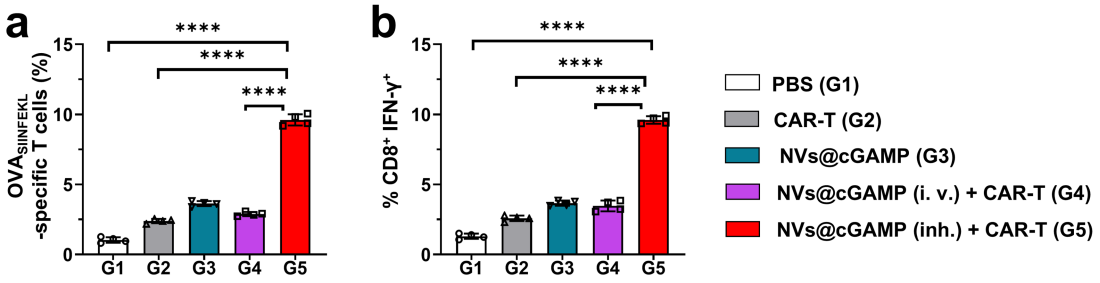

Supplementary Figure 27. (a) In LLC-MSLN-OVA tumor-bearing mice, the percentage of OVA $_{(SIINFEKL)}$-specific $CD8^+$ T cells in the spleen was assessed *via* flow cytometry after various treatments. (b) Following stimulation with OVA peptides, the percentage of T cells producing IFN-γ within the $CD8^+$ T cell population was analyzed across different treatment groups. Data are presented as the mean ± S.D. ***$p \leq 0.001$, ****$p \leq 0.0001$ by one-way ANOVA with Tukey's post-test for (a) and (b).

Q: *19. In line 417 and line 430, the authors concluded that NVs@cGAMP enhanced CAR-T cell immune memory. I recommend that the authors detect the memory phenotype of CAR-T cells by using specific markers such as CD45RO, CD62L, and CCR7 to gain deeper insights into the memory T cell response. Incorporating these analyses will provide a more comprehensive validation of the impact of NVs@cGAMP on CAR-T cell immune memory.*

R: Thank you for your insightful suggestion. We fully agree that detecting the memory phenotype of CAR-T cells is essential to gain deeper insights into the impact of NVs@cGAMP on CAR-T cell immune memory.

In human studies, memory T cell subsets are typically distinguished using markers such as CD45RO, CD62L, and CCR7. However, in murine models, CD44 and CD62L are the standard markers used to differentiate memory T cell subsets[32, 33]. Therefore, in our study, we employed CD44 and CD62L to identify memory CAR-T cells within tumor tissues. Our results demonstrated that the group treated with aerosolized NVs@cGAMP in combination with CAR-T cells exhibited significantly higher proportions of central memory T cells and effector memory T cells compared to other treatment groups (**Fig. 7i**). This increase in memory T cell populations is beneficial for maintaining the long-term anti-tumor efficacy of CAR-T cells, as memory T cells are crucial for sustained immune surveillance and rapid response upon tumor recurrence.

We have incorporated these updated results and the corresponding discussion into the revised manuscript. The updated figures illustrating these findings are as follows:

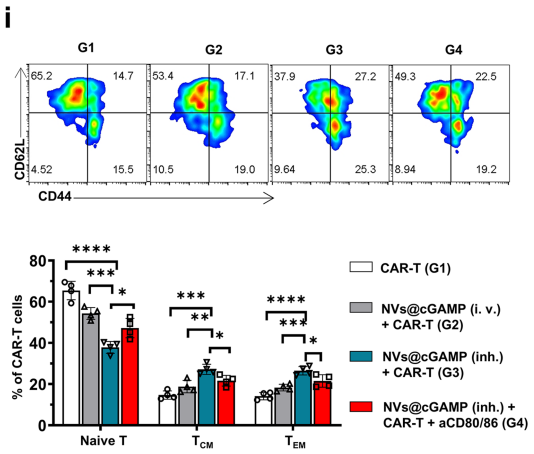

Figure 7. (i) Representative flow cytometry plots and statistical analysis of naïve T cells, central memory T cells (T_{CM}), and effector memory T cells (T_{EM}) within the CAR-T cell population in the TME across different treatment groups (n = 4).

Q: *Minor concerns: 1. In figure 2c, the authors utilized flow cytometry to quantify the CAR protein on the T cell surface. It is essential that the method for detecting the CAR protein on the T cell surface be thoroughly explained in the method section to ensure transparency and reproducibility of the experimental procedures.*

R: Thank you for your valuable suggestion. We have added a detailed description of the method used to detect the CAR protein on the T cell surface in the revised manuscript, as follows:

"The expression efficiency of the CAR protein on T cells was analyzed by flow cytometry. Specifically, T cells transduced for 7 days were washed with PBS and resuspended. We then incubated 1×10^6 cells with 1 μL of Protein L (1 mg/mL) at 4°C for 30 minutes. Protein L binds specifically to the kappa light chain of the scFv region in the CAR construct, enabling the detection of CAR expression. After incubation, the cells were washed three times with PBS containing 1% bovine serum albumin (BSA). The samples were then stained with PE-conjugated streptavidin (BioLegend, San Diego, CA, USA) and washed three more times.

Finally, the cells were analyzed using a CytoFLEX LX flow cytometer (Beckman Coulter, Atlanta, GA, USA)."

We hope that this detailed methodology enhances the clarity and reproducibility of our experimental procedures.

Q: *2. In figure 2e-f, it would greatly improve the comparative analysis to display the statistical differences between each group, providing clearer insight into the observed variations.*

R: Thank you for your valuable suggestion. In the revised manuscript, we have added the statistical differences between each group in Figures 2e-f to provide clearer insights into the observed variations.

Q: *3. In figure 1e, 1f, 1l, 1m, 2j, 5n, 6c, 6e, 6f, 8c and 8f, statistical analysis should be performed for comprehensive data evaluation.*

R: Thank you very much for your insightful suggestion. Following your recommendation, we have updated the figures you mentioned, as well as the newly added figures, to include the statistical differences between each group.

Q: *4. In figure 8 and line 1017, the authors stated that all data are presented as mean ± S.D. However, it's important to highlight that only figure 8f follows this format. Therefore, I recommend revising line 1017 to ensure that the statement aligns with how the data are presented in the figure.*

R: Thank you for your valuable suggestion. We have removed the original statement in line 1017 to prevent any confusion. Additionally, we have revised the legend of Figure 8h (formerly Figure 8f in the original manuscript) to read:

"Changes in tumor volume in naive mice and mice cured by combination therapy after injection into the inguinal region with LLC or LLC-MSLN cells in the LLC model (left panel), and with B16 or B16-MSLN cells in the B16 model (right panel) (n = 4). Data are presented as mean ± S.D."

Reviewer #4 *(Remarks to the Author): with expertise in drug delivery, cancer therapy*

Q: *In this study, the authors have designed a STING agonist (cGAMP) delivery strategy to improve CAR-T cell therapy. They used nanovesicles displaying anti-PDL-1 (aPDL-1-scFv) and loaded with STING agonist (cGAMP) as a strategy for this approach. They adopted intranasal delivery to target pulmonary immune responses, which could modulate immunosuppressive tumor microenvironment and enhance CAR-T cell accumulation in the tumor to improve therapeutic outcome. The study evaluated Mesothelin (MSLN) targeted CAR-T cells along with the aPDL-1 scFV engineered nanovesicle constructed from the cell membrane of 293T cells stably expressing aPD-L1-scFv for the study. The study initially evaluated MSLN-CAR-T against lung tumor developed using intravenous injection of B16-lung cancer cells and found a partial treatment response, which was further evaluated by combining with cGAMP loaded aPD-L1-NVs or as a mixture of cGAMP with aPD-L1-NVs with CAR-T cells to monitor the enhanced treatment outcome. The results found that when MSLN-CAR-T cells were combined with cGAMP loaded aPD-L1-NVs, the treatment outcome significantly improved. The study was well designed, and the results outcome are reasonably good but need further long-term validation to understand the potential application of this strategy to the next level in the clinic. There are several other important experiments need to be conducted to address for further validation of this research and treatment outcome. The manuscript can be considered for publication after addressing the following major concerns.*

R: Thank you very much for your positive comments. Your feedback has been immensely valuable in improving the quality of our work. Please find the following point-to-point responses to your comments and suggestions.

Q: *1. The measured zeta potential (Figure 3) of Free NVs is different from aPDL-1 NV. Please explain or perform another experiment where reconstruct Free NVs using aPD-L1 scFV and measure zeta potential. The expression of a single protein on the cell membrane will not provide this much change in the charge.*

R: Thank you very much for your constructive comments. Indeed, we share your surprise regarding the change in zeta potential of the nanovesicles before and after modification. We appreciate your suggestion to reconstruct Free NVs using aPD-L1 scFv and measure the zeta potential. However, reconstructing aPD-L1 scFv on Free NVs would require the introduction of additional molecules or linkers, which could complicate the direct analysis of how aPD-L1 scFv affects the zeta potential of nanovesicles. Therefore, we sought to explain this phenomenon through literature research.

Upon reviewing numerous studies on the changes in zeta potential before and after antibody or scFv modification of nanoparticles, we found that this change may be

related to the isoelectric point (pI) and the quantity of the antibody (or scFv) modified on the nanoparticle surface.

The isoelectric point (pI) of an antibody (or scFv) depends on its amino acid composition, particularly the charged residues. If the pH of the surrounding environment is below the pI of the antibody (or scFv), the molecule carries a net positive charge; conversely, if the pH is above the pI, the antibody will carry a net negative charge[34, 35]. In our study, the calculated pI of aPD-L1 scFv is approximately 8.8 (as determined using the ExPASy Compute pI/Mw tool: https://web.expasy.org/compute_pi/), which means that in PBS solution (pH ~7.4), the aPD-L1 scFv is positively charged. The positive charges of the aPD-L1 scFv can partially neutralize the negative charges on the surface of the nanovesicles, resulting in an increase in the zeta potential by about 5 mV. Since different antibodies or scFvs have different isoelectric points, the changes in zeta potential upon their modification can vary significantly. For example, previous studies have reported that the zeta potential of exosomes and AuNP increased by approximately 6 mV and 18 mV, respectively, after coupling or expressing anti-PD-L1 scFv[36, 37]. In contrast, the zeta potential of exosomes decreased by about 8.5 mV after coupling with anti-VEGFR antibodies[38].

Additionally, the amount of antibody or scFv conjugated or expressed on the nanoparticles significantly affects the overall surface charge. If only a small amount of antibody or scFv is attached, the overall charge of the nanoparticles may not change markedly. However, when a large amount is conjugated or expressed, substantial changes in the zeta potential can occur.

We acknowledge that the factors affecting the zeta potential of nanovesicles are complex and multifaceted. We plan to further investigate this phenomenon through additional literature research and experiments in future studies. We greatly appreciate your insightful feedback, which provides valuable guidance for the optimization of nanovesicle modifications.

Q: *2. Figure 3l describing INF-beta secretion by DCs upon incubation with STING-NVs is misleading. The data does not explain what they have claimed in the manuscript.*

R: Thank you for your insightful comments on Figure 3l. We apologize for any confusion caused by the original presentation of our data. The main purpose of this experiment was to evaluate the long-term storage stability of aPD-L1 NVs@cGAMP. Specifically, we assessed whether these nanovesicles maintain their bioactivity over time by comparing the levels of IFN-β secretion induced in dendritic cells (DCs) by stored versus freshly prepared aPD-L1 NVs@cGAMP (Day 0). To this end, we stored aPD-L1 NVs@cGAMP at -80°C and retrieved samples on days 5, 15, 30, and 60. After co-incubating them with DCs for 12 hours, we measured IFN-β secretion using an ELISA assay.

We understand that the original presentation of **Figure 3l** and the corresponding text may not have fully conveyed the significance of this experiment. To address your concerns, we have made the following revisions: (1) DC group treated with PBS or aPD-L1 NVs has been included in the revised Figure 3l to provide a clear representation of the basal level of IFN-β secretion. (2) Statistical comparisons between IFN-β levels induced by freshly prepared and stored aPD-L1 NVs@cGAMP have been added, effectively demonstrating the preservation of bioactivity over time. (3) The annotations on Figure 3l have been refined to more clearly convey the intended information. (4) The figure legend has been improved for greater clarity and completeness. (5) The manuscript's description of Figure 3l has been updated to align with the revised figure.

We appreciate your feedback and hope these adjustments address your concerns. Please do not hesitate to let us know if you have any further suggestions, and we will be happy to make the necessary changes.

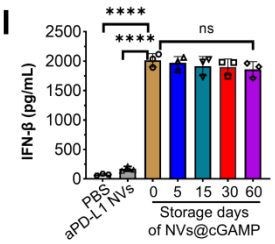

Figure 3. (l) Efficiency of aPD-L1 NVs@cGAMP in inducing IFN-β release from DCs after storage at –80 °C for varying durations. DCs treated with PBS and aPD-L1 NVs were used as negative controls (n = 3).

Q: *3. STING agonist is important for activating immunosuppressive phenotype while aPD-L1-NV is important for blocking STING mediated upregulation of PD-L1 expression (Figure 4). This can happen either delivered using loaded NVs or STING+NV codelivery. What could be reason the codelivery is showing differential effect compared to loaded NVs? Please explain in the manuscript discussion.*

R: Thank you for highlighting this important issue. Before addressing the underlying mechanisms, we would first like to correct an error in the original manuscript due to our oversight. In Figures 4a, 4c, and 4e, we incorrectly labeled the group "cGAMP + aPD-L1 NVs" (co-administration of aPD-L1 NVs with free STING agonist) as "NVs@cGAMP + aPD-L1 NVs." In the revised manuscript, this has been corrected to "cGAMP + aPD-L1 NVs."

Regarding the differential effects observed, aPD-L1 NVs@cGAMP (STING agonist loaded into NVs) outperform the cGAMP + aPD-L1 NVs (co-delivery) group in promoting inflammatory cytokine release. This difference may be attributed to enhanced cellular uptake and retention of the STING agonist when encapsulated in nanovesicles. Generally, STING agonists are hydrophilic and negatively charged, which limits their ability to penetrate cell membranes and results in poor cellular uptake. Additionally, free STING agonists are prone to degradation by phosphodiesterases in circulation and on the cell surface, leading to a shorter half-

life[5, 8, 9]. In contrast, nanovesicles, with their lipid bilayer structure, can facilitate rapid cellular entry, thereby improving the intracellular delivery and retention of STING agonists[9]. This phenomenon has been previously demonstrated in studies such as that by Kathleen M et al., where STING agonist-loaded extracellular vesicles exhibited a tenfold increase in cellular uptake compared to free STING agonists[8].

We have incorporated this explanation into the revised manuscript to clarify the observed results as follows:

TNF-α secretion enhancement. This synergistic effect may be attributed to aPD-L1 NVs facilitating the cellular uptake of STING agonists. Typically, STING agonists are hydrophilic and negatively charged, which limits their ability to penetrate cell membranes and results in poor cellular uptake[48, 49]. Moreover, free STING agonists are readily degraded by phosphodiesterases on the cell surface and in circulation, leading to a short half-life[50]. In contrast, nanovesicles with lipid bilayer structures can facilitate rapid entry into cells via endocytosis or membrane fusion, thereby improving the intracellular delivery and retention of STING agonists[51]. Studies by Kathleen M. et al. have demonstrated that loading STING agonists into extracellular vesicles increased cellular uptake tenfold compared to free STING agonists[49].

Q: *4. Please explain in the results or figure legends the cell types used in each experiment. For example, cGAMP-NVs dose dependently enhance INF-beta secretion---in what cells. It would be easy for the readers to understand the results without going back and forth into the methods section.*

R: Thank you for your valuable suggestion. Per your suggestion, we have added a description of the cell types used in each experiment in the figure legends, particularly in **Fig. 4b**, where we illustrate the dose-dependent enhancement of INF-β secretion by cGAMP-NVs. Additionally, we have also clarified the cell types used in **Fig. 4d and Fig. 4f** for greater transparency and ease of understanding.

Q: *5. The study claims that combination of aPD-L1 targeted cGAMP loaded NVs along with MSLN-CAR-T improves treatment outcome, but the survival curve results shows that only a slight improvement rather not achieving disease free outcome.*

R: Thank you for pointing out this issue. We apologize for any confusion caused by the presentation of our results. In fact, our data demonstrate that the CAR-T + NVs@cGAMP group (the combination of aPD-L1-targeted cGAMP-loaded NVs and MSLN-CAR-T) achieved 100% survival in mice by day 50 post-treatment, indicating a significant improvement in therapeutic efficacy.

To make this clearer, we have included statistical analysis between the groups in the figure, highlighting the improvement in the CAR-T + NVs@cGAMP group. As depicted in the survival curve, the mice in this group (G6, represented by the topmost red line in the Fig. 6f) achieved 100% survival by day 50 post-treatment.

We hope this explanation and the revisions will address your concerns.

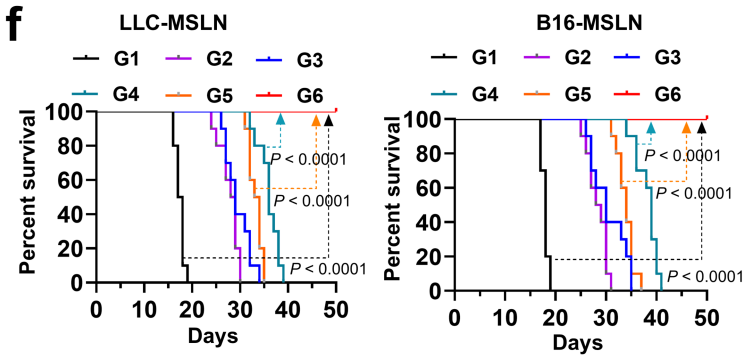

Figure 6. (f) Survival curves of mice treated with different agents in both tumor models (n = 10). ****$p \leq 0.0001$ by log rank (Mantel-Cox) test for (f).

Q: *6. The entire study is conducted using a single B16 tumor model. It is better to address the efficacy of this treatment approach in another lung cancer model.*

R: We fully agree with your suggestion. In fact, Reviewer 3 also recommended using the LLC cell line (a murine Lewis lung carcinoma cell line) to evaluate the effectiveness of our cancer treatment strategy. Therefore, we have included data demonstrating the efficacy of CAR-T cells combined with aPD-L1 NVs@cGAMP in both the B16 and LLC tumor models in the revised manuscript. The corresponding results have been added to **Figures 5, 6, 7, and 8**. Among them, the most relevant findings to evaluate the efficacy of our treatment strategy have been added to **Figure 6**, as follows:

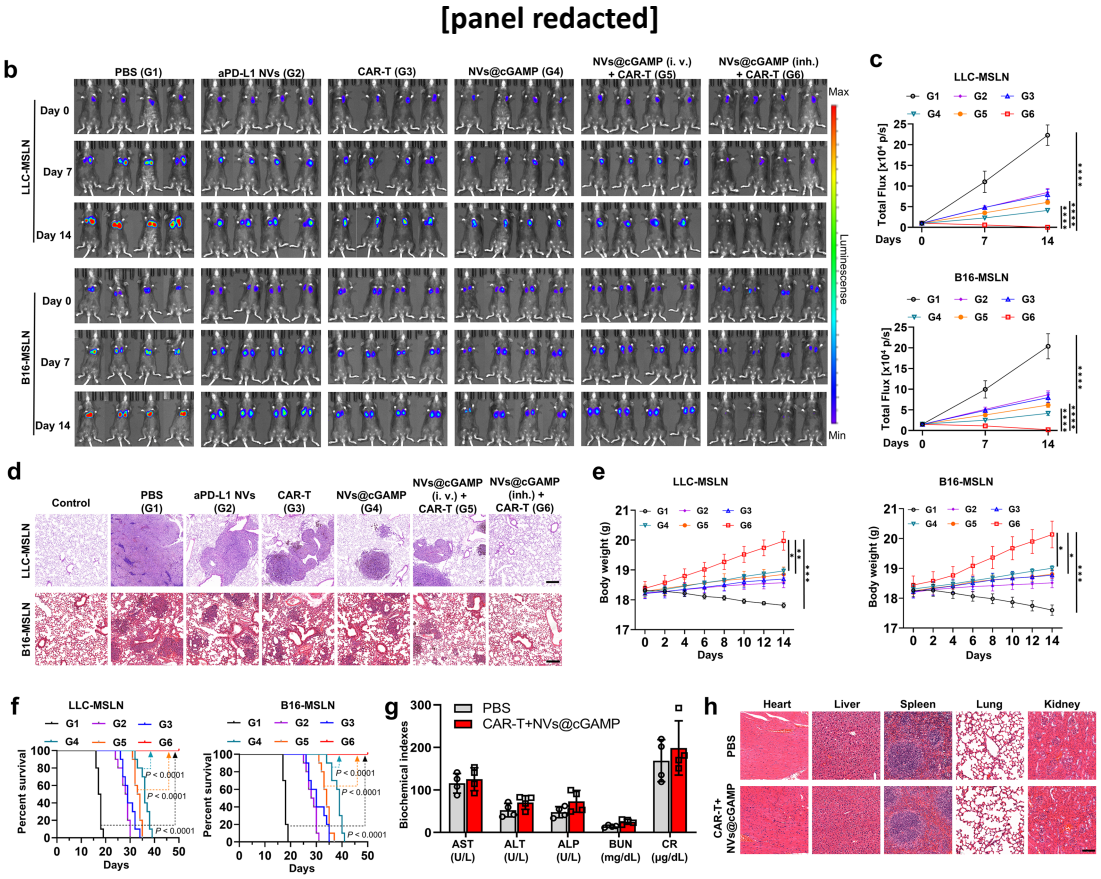

Figure 6. Enhancement of the antitumor capacity of CAR-T cells by aPD-L1 NVs@cGAMP. (a) Schematic illustration of aPD-L1 NVs@cGAMP augmenting CAR-T cell anti-tumor efficacy. (b-c) Bioluminescence was measured by the IVIS system to evaluate tumor growth in the different treatment groups, and the bioluminescence intensity was statistically analyzed (n = 4). (d) Representative images of H&E-stained sections from LLC-MSLN and B16-MSLN tumor-bearing mice in various treatment groups. (e) Body weight change curves of mice treated with different agents in both tumor models (n = 4). (f) Survival curves of mice treated with different agents in both tumor models (n = 10). (g) Serum biochemical indices of mice receiving PBS or combined treatment with CAR-T cells and aPD-L1 NVs@cGAMP (n = 4). (h) Representative lung images and H&E-stained sections of mice receiving PBS or combined treatment with CAR-T cells and aPD-L1 NVs@cGAMP. Scale bar: 100 μm. All the data are presented as the mean ± S.D. *$p \leq 0.05$, **$p \leq 0.01$, ***$p \leq 0.001$ and ****$p \leq 0.0001$ by two-way ANOVA with Tukey's post-test for (c) and (e); and by log rank (Mantel-Cox) test for (f).

Thank you for your insightful suggestion, which has further enhanced the reliability of our study's findings.

Q: *7. The endothelial anergy and tumor vascular expression of PD-L1 is linked with tumor targeted CAR-T and immune checkpoint blockade therapies. Please show some immunostaining results of lung tumor for vascular expression of PD-L1 after different treatments by co-staining with CD31 and PD-L1 targeted antibodies.*

R: Thank you for your valuable suggestion. Indeed, endothelial anergy within tumor tissues leads to the downregulation of adhesion molecules and chemokines on

vascular endothelial cells, thereby hindering the recruitment and extravasation of CAR-T cells to the tumor site[39, 40]. Additionally, the expression of PD-L1 on the tumor vasculature can suppress the activity of T cells attempting to infiltrate the tumor microenvironment, further facilitating immune evasion by tumor cells[41, 42].

In our study, nanovesicle-loaded STING agonists were employed to reduce endothelial anergy by upregulating chemokines and adhesion molecules, enhancing immune cell infiltration. However, STING activation also induces high expression of PD-L1 on the tumor vasculature as part of an immunosuppressive feedback mechanism[4, 43]. Therefore, as you correctly pointed out, evaluating PD-L1 expression in tumor tissues is of significant importance.

Per your suggestion, we performed immunostaining of lung tumor tissues treated with different therapies, utilizing co-staining with CD31 and PD-L1 antibodies analyzed *via* confocal microscopy. As shown in **Supplementary Figure 22**, lung tumor tissues treated with cGAMP exhibited high PD-L1 expression in both tumor cells and the tumor vasculature. In contrast, treatment with aPD-L NVs led to a dramatic decrease in detectable PD-L1 expression within tumor cells and vasculature, indicating that aPD-L NVs effectively block PD-L1 in the tumor microenvironment. Importantly, the combination treatment group of aPD-L NVs@cGAMP with CAR-T cells showed only minimal PD-L1 expression, suggesting that aPD-L NVs@cGAMP successfully blocks STING agonist-induced PD-L1 expression, thereby preventing CAR-T cell exhaustion.

We have included the corresponding results in **Supplementary Figure 22**, and the results are discussed in the revised manuscript. Thank you once again for your valuable feedback, which has significantly strengthened our manuscript.

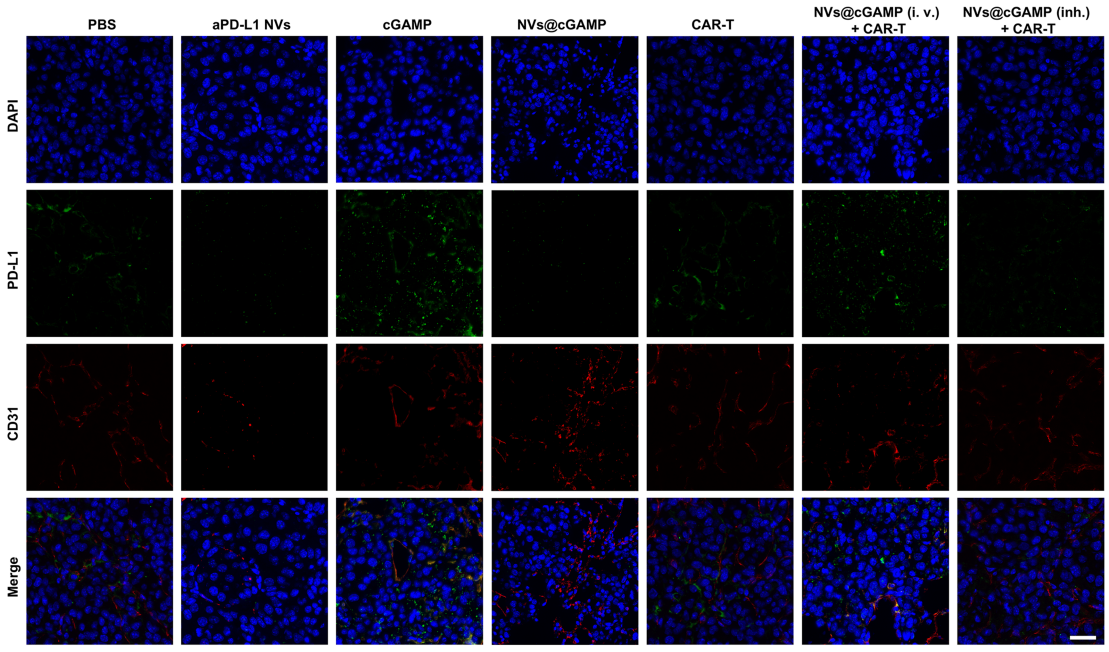

Supplementary Figure 22. Following different treatments of LLC-MSLN tumor-bearing mice, co-expression of CD31 (red) and PD-L1 (green) in tumor tissues was analyzed by confocal microscopy, with CD31 serving as a vascular marker. Scale bar: 50 μm.

Q: *8. It is also important to show the amount of CAR-T cells presence after the completion of treatment to correlate the results with the treatment outcome in different groups by ex vivo histology of tumor and the spleen.*

R: Thank you for your insightful suggestion. In response, we sacrificed the mice at the end of the treatment and prepared histological sections of their lungs and spleens. We utilized confocal microscopy to observe and quantify the number of CAR-T cells infiltrating the tumor tissues and spleens. As shown in **Supplementary Figure 20**, the group treated with inhaled NVs@cGAMP combined with CAR-T therapy exhibited a significantly higher accumulation of CAR-T cells in both the spleen and residual tumor tissues compared to other treatment groups. This increase in CAR-T cell infiltration correlates with the improved survival rates observed in the NVs@cGAMP (inh.) + CAR-T group.

We have included these results in **Supplementary Figure 20** of the revised manuscript to provide a clearer correlation between CAR-T cell presence and treatment outcomes.

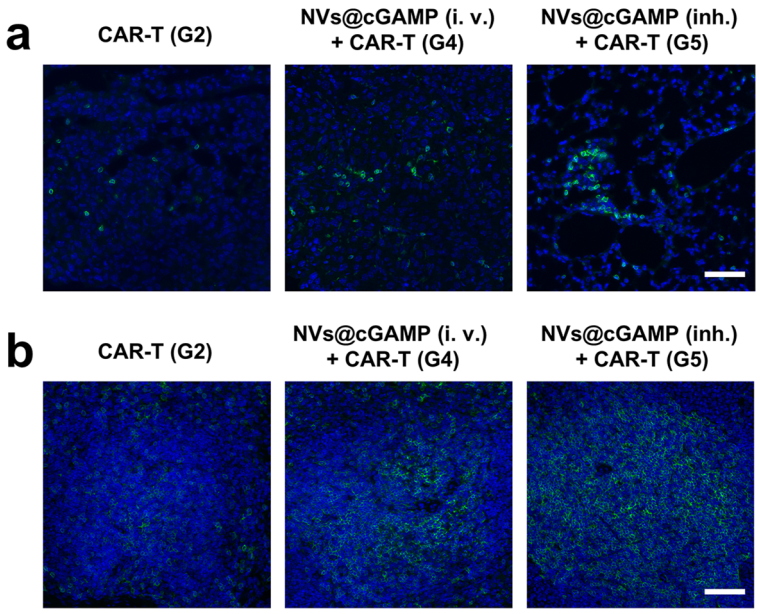

Supplementary Figure 20. Infiltration of CAR-T cells in tissues. (a) After different treatments were administered to LLC-MSLN tumor-bearing mice, CAR-T cell infiltration in tumor tissues was observed using confocal microscopy. Scale bar: 50 μm. (b) After different treatments were administered to LLC-MSLN tumor-bearing mice, CAR-T cell infiltration in spleens was observed using confocal microscopy. Scale bar: 100 μm.

Q: *9. Figure 8, the tumor cell imaging immediately after implantation into inguinal region of the mouse is needed. The initial amount of implant is important for further tumor growth.*

R: We sincerely appreciate your valuable feedback. In response to your feedback, we have revised the manuscript to include the fluorescence imaging performed immediately after the tumor cells were implanted in the inguinal region of the mice, which is now incorporated into **Figure 8h**.

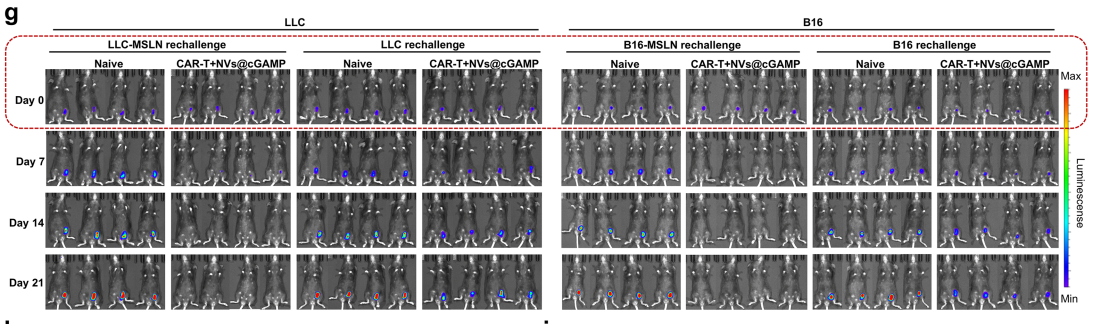

Figure 8. (g) In both tumor models, after re-inoculating either the parental tumor cells (LLC or B16) or their MSLN-expressing counterparts (LLC-MSLN or B16-MSLN) in the groin of naive mice and those cured by the combined therapy, bioluminescence intensity was measured using the IVIS system to evaluate tumor recurrence (*n*=4).

References

1. Kimiz-Gebologlu I, Oncel SS. Exosomes: Large-scale production, isolation, drug loading efficiency, and biodistribution and uptake. *J Control Release* **347**, 533-543 (2022).

2. Zhang E, Phan P, Zhao Z. Cellular nanovesicles for therapeutic immunomodulation: A perspective on engineering strategies and new advances. *Acta Pharm Sin B* **13**, 1789-1827 (2023).

3. Mondal J, *et al.* Hybrid exosomes, exosome-like nanovesicles and engineered exosomes for therapeutic applications. *J Control Release* **353**, 1127-1149 (2023).

4. Zhu Y, An X, Zhang X, Qiao Y, Zheng T, Li X. STING: a master regulator in the cancer-immunity cycle. *Mol Cancer* **18**, 152 (2019).

5. Zhao K, Huang J, Zhao Y, Wang S, Xu J, Yin K. Targeting STING in cancer: Challenges and emerging opportunities. *Biochim Biophys Acta Rev Cancer* **1878**, 188983 (2023).

6. Wu JJ, Zhao L, Hu HG, Li WH, Li YM. Agonists and inhibitors of the STING pathway: Potential agents for immunotherapy. *Med Res Rev* **40**, 1117-1141 (2020).

7. Huang C, *et al.* Overcoming challenges in the delivery of STING agonists for cancer immunotherapy: A comprehensive review of strategies and future perspectives. *Mater Today Bio* **23**, 100839 (2023).

8. McAndrews KM, Che SPY, LeBleu VS, Kalluri R. Effective delivery of STING agonist using exosomes suppresses tumor growth and enhances antitumor immunity. *J Biol Chem* **296**, 100523 (2021).

9. Jang SC, *et al.* ExoSTING, an extracellular vesicle loaded with STING agonists, promotes tumor immune surveillance. *Commun Biol* **4**, 497 (2021).

10. Li YJ, *et al.* Artificial exosomes for translational nanomedicine. *J Nanobiotechnology* **19**, 242 (2021).

11. Garcia-Fernandez J, Fuente Freire M. Exosome-like systems: Nanotechnology to overcome challenges for targeted cancer therapies. *Cancer Lett* **561**, 216151 (2023).

12. Moghassemi S, *et al.* Extracellular vesicles in nanomedicine and regenerative medicine: A review over the last decade. *Bioact Mater* **36**, 126-156 (2024).

13. Wang K, *et al.* Milk-derived exosome nanovesicles: recent progress and daunting hurdles. *Crit Rev Food Sci Nutr*, 1-16 (2024).

14. He S, Zhao Z. Genetically engineered cell-derived nanovesicles for cancer immunotherapy. *Nanoscale* **16**, 8317-8334 (2024).

15. Guerin MV, Finisguerra V, Van den Eynde BJ, Bercovici N, Trautmann A. Preclinical murine tumor models: a structural and functional perspective. *Elife* **9**, (2020).

16. Barutello G, *et al.* Strengths and Weaknesses of Pre-Clinical Models for Human Melanoma Treatment: Dawn of Dogs' Revolution for Immunotherapy. *Int J Mol Sci* **19**, (2018).

17. Patton EE, *et al.* Melanoma models for the next generation of therapies. *Cancer Cell* **39**, 610-631 (2021).

18. Overwijk WW, Restifo NP. B16 as a mouse model for human melanoma. *Curr Protoc Immunol* **Chapter 20**, Unit 20 21 (2001).

19. Hanada KI, Yu Z, Chappell GR, Park AS, Restifo NP. An effective mouse model for adoptive cancer immunotherapy targeting neoantigens. *JCI Insight* **4**, (2019).

20. Danciu C, *et al.* A characterization of four B16 murine melanoma cell sublines molecular fingerprint and proliferation behavior. *Cancer Cell Int* **13**, 75 (2013).

21. Miller TJ, Anyaegbu CC, Lee-Pullen TF, Spalding LJ, Platell CF, McCoy MJ. PD-L1+ dendritic cells in the tumor microenvironment correlate with good prognosis and CD8+ T cell infiltration in colon cancer. *Cancer Sci* **112**, 1173-1183 (2021).

22. Li G, *et al.* cGAS-STING pathway mediates activation of dendritic cell sensing of immunogenic tumors. *Cell Mol Life Sci* **81**, 149 (2024).

23. Eric H, *et al.* High expression of PD-L1 on conventional dendritic cells in tumour-draining lymph nodes is associated with poor prognosis in oral cancer. *Cancer Immunol Immunother* **73**, 165 (2024).

24. Xu N, *et al.* STING agonist promotes CAR T cell trafficking and persistence in breast cancer. *J Exp Med* **218**, (2021).

25. Wang-Bishop L, *et al.* STING-activating nanoparticles normalize the vascular-immune interface to potentiate cancer immunotherapy. *Sci Immunol* **8**, eadd1153 (2023).

26.Chin EN, Sulpizio A, Lairson LL. Targeting STING to promote antitumor immunity. *Trends Cell Biol* **33**, 189-203 (2023).

27. Le Naour J, Zitvogel L, Galluzzi L, Vacchelli E, Kroemer G. Trial watch: STING agonists in cancer therapy. *Oncoimmunology* **9**, 1777624 (2020).

28. Lai J, *et al.* Adoptive cellular therapy with T cells expressing the dendritic cell growth factor Flt3L drives epitope spreading and antitumor immunity. *Nat Immunol* **21**, 914-926 (2020).

29. Jin C, Ma J, Ramachandran M, Yu D, Essand M. CAR T cells expressing a bacterial virulence factor trigger potent bystander antitumour responses in solid cancers. *Nat Biomed Eng* **6**, 830-841 (2022).

30. Conde E, *et al.* Epitope spreading driven by the joint action of CART cells and pharmacological STING stimulation counteracts tumor escape via antigen-loss variants. *J Immunother Cancer* **9**, (2021).

31. Karandikar SH, Sidney J, Sette A, Selby MJ, Korman AJ, Srivastava PK. New epitopes in ovalbumin provide insights for cancer neoepitopes. *JCI Insight* **5**, (2019).

32. Adachi K, Kano Y, Nagai T, Okuyama N, Sakoda Y, Tamada K. IL-7 and CCL19 expression in CAR-T cells improves immune cell infiltration and CAR-T cell survival in the tumor. *Nat Biotechnol* **36**, 346-351 (2018).

33. Evgin L, *et al.* Oncolytic virus-mediated expansion of dual-specific CAR T cells improves efficacy against solid tumors in mice. *Sci Transl Med* **14**, eabn2231 (2022).

34. Liu S, Verma A, Kettenberger H, Richter WF, Shah DK. Effect of variable domain charge on in vitro and in vivo disposition of monoclonal antibodies. *MAbs* **13**, 1993769 (2021).

35. Gupta P, Makowski EK, Kumar S, Zhang Y, Scheer JM, Tessier PM. Antibodies with Weakly Basic Isoelectric Points Minimize Trade-offs between Formulation and Physiological Colloidal Properties. *Mol Pharm* **19**, 775-787 (2022).

36. Li X, *et al.* Genetically Programmable Vesicles for Enhancing CAR-T Therapy against Solid Tumors. *Adv Mater* **35**, e2211138 (2023).

37. Emami F, *et al.* Doxorubicin and Anti-PD-L1 Antibody Conjugated Gold Nanoparticles for Colorectal Cancer Photochemotherapy. *Mol Pharm* **16**, 1184-1199 (2019).

38. Tian Y, *et al.* Reduction of choroidal neovascularization via cleavable VEGF antibodies conjugated to exosomes derived from regulatory T cells. *Nat Biomed Eng* **5**, 968-982 (2021).

39. Wachholz GE, Akbari P, Huijbers EJM, Jalan P, van Beijnum JR, Griffioen AW. Targeting endothelial cell anergy to improve CAR T cell therapy for solid tumors. *Biochim Biophys Acta Rev Cancer* **1879**, 189155 (2024).

40. Fang J, *et al.* Exploring the crosstalk between endothelial cells, immune cells, and immune checkpoints in the tumor microenvironment: new insights and therapeutic implications. *Cell Death Dis* **14**, 586 (2023).

41. Yamaguchi Y, *et al.* PD-L1 blockade restores CAR T cell activity through IFN-gamma-regulation of CD163+ M2 macrophages. *J Immunother Cancer* **10**, (2022).

42. Lanitis E, Irving M, Coukos G. Targeting the tumor vasculature to enhance T cell activity. *Curr Opin Immunol* **33**, 55-63 (2015).

43. Yang H, *et al.* STING activation reprograms tumor vasculatures and synergizes with VEGFR2 blockade. *J Clin Invest* **129**, 4350-4364 (2019).

Point-by-Point Response

NOTE: The comments are in italic black font, and our responses are in normal blue font. "Q" is short for "Question" and "R" is short for "Response".

Response to Comments from Reviewers

Reviewer #1 (Remarks to the Author):

Q: *The authors have addressed my comments.*

R: Thank you very much for your positive feedback and recognition of our work.

Reviewer #2 (Remarks to the Author):

Q: *he authors have done a decent job addressing my comments. I think the question of whether this type of preclinical study in the mouse, with its acknowledged limitations, is valuable enough to warrant publication in Nature Comm. is, it seems to me, an editorial decision.*

R: We sincerely appreciate your positive evaluation of our revised manuscript.

Reviewer #3 (Remarks to the Author):

Q: *The authors have addressed most of my comments, but there are still some issues regarding rigor and unresolved mysteries in the manuscript.*

R: Thank you for recognizing our revision work and for your constructive suggestions. We sincerely appreciate your efforts to improve the quality of our manuscript. Please find the following point-to-point responses to your comments and suggestions.

Q: *1. The authors have further demonstrated antitumor effects of MSLN CAR-T cells in LLC tumor models. However, only four mice were used in the group infused with the CAR-T cells in this experiment. In addition, the authors need to specify how many times the animal experiment has been repeated.*

R: Thank you for pointing out this important issue. In this study, we included 4 mice per group when evaluating tumor growth using the IVIS imaging system, and 10 mice per group when assessing the survival rates of tumor-bearing mice under different treatment regimens. As you correctly indicated, appropriate sample size is crucial in animal experiments to ensure reliable and statistically significant results while adhering to ethical guidelines[1]. Therefore, we carefully determined our sample sizes by adhering to the 3R principles (Replacement, Reduction, Refinement) and conducting statistical power analyses.

For the IVIS imaging experiments, where bioluminescence values are continuous variables[2], we calculated the sample size by specifying a power of 80%, a significance level of 0.05, the expected mean difference, and the standard deviation of the overall mean. Based on calculations using online sample size calculators (https://eda.nc3rs.org.uk/; https://www.bu.edu/research/forms-policies/iacuc-sample-size-calculations/), setting the number of mice at 4 per group was deemed reasonable for the IVIS imaging experiments. For the survival rate analysis[2, 3], which involves dichotomous variable outcomes, we calculated the required sample size using formulas appropriate for proportions. By combining these calculations with the resource equation approach and considering experimental designs from previous literature[4, 5, 6, 7, 8], we set the sample size at 10 mice per group for the survival analyses.

Regarding experimental repeats, we included biological replicates to reduce bias due to individual differences. In our study, each mouse within a group received the same but independent treatment, making each mouse a biological replicate. Therefore, in the IVIS imaging experiments and survival rate analyses, we effectively had 4 and 10 biological replicates, respectively. We have now specified the number of experimental repeats in the revised manuscript.

Q: *2. The authors suggested that CXCL9 and CXCL10 were upregulated in aPD-L1 NVs@cGAMP-MSLN CAR-T cells. However, they did not characterize and provide evidence on whether these CAR-T cells infiltrated into tumors, such as through IHC assays or immunofluorescence (IF).*

R: Thank you for your valuable suggestion. We fully agree that it is crucial to evaluate whether CAR-T cell infiltration into tumor tissues has increased following treatment, especially since our data show that aPD-L1 NVs@cGAMP promotes the upregulation of CXCL9 and CXCL10 mRNA levels in tumor tissues **(Fig. 5a)**. CXCL9 and CXCL10 are soluble chemokines secreted by various cell types, including leukocytes, epithelial cells, endothelial cells, and stromal cells. These chemokines are well-known for their role in recruiting $CD8^+$ T cells, including CAR-T cells, to the tumor microenvironment[9, 10, 11]. In fact, in our first revision, Reviewer 4 also suggested that we evaluate whether our therapeutic strategy enhances CAR-T cell infiltration in tumor tissues through immunofluorescence techniques. In response, we have already used immunofluorescence techniques to detect the infiltration of CAR-T cells in tumor tissues.

Briefly, after sacrificing the mice at the end of the treatment and preparing their lung tissue sections, we stained the sections with an FITC-conjugated anti-GFP antibody (Abcam, ab6662) to specifically label the CAR-T cells expressing GFP. We then used confocal microscopy to observe the infiltrating CAR-T cells within the tumor microenvironment. As shown in **Supplementary Figure 20**, the group treated with inhaled aPD-L1 NVs@cGAMP combined with CAR-T therapy exhibited a significantly higher accumulation of CAR-T cells in the residual tumor tissues compared to other treatment groups. The increased infiltration of CAR-T

cells may be partly attributed to the upregulated CXCL9 and CXCL10 in the tumor microenvironment.

We have included these results in **Supplementary Figure 20** of the revised manuscript, as follows:

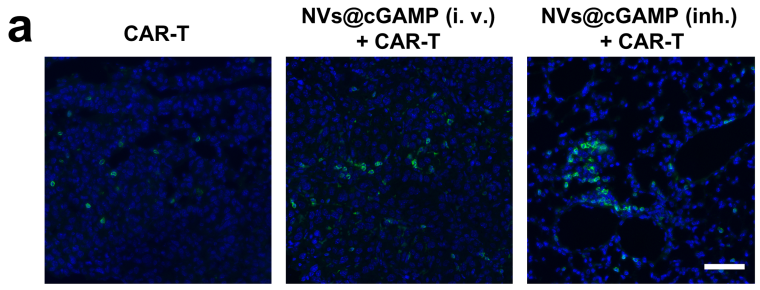

Supplementary Figure 20. Infiltration of CAR-T cells in tissues. (a) After different treatments were administered to LLC-MSLN tumor-bearing mice, CAR-T cell infiltration in tumor tissues was observed using confocal microscopy. Scale bar: 50 μm.

Q: *3. The authors showed that treatment with aPD-L1 NVs@cGAMP increased the presence of T helper 1 (Th1) and Th17 cells, while reduced the number of Th2 cells in the tumor microenvironment (Fig. 5g and Fig. 5i). However, they did not explain why these changes happened. Were these phenotypes caused by the blockage of PD-L1 or TGF-β1? The authors should provide a discussion to clarify these results.*

R: Thank you for your insightful suggestions. The regulation of Th1, Th2, and Th17 cell populations within the tumor microenvironment (TME) is indeed a complex process influenced by various cytokines and cellular interactions[12]. Cytokines such as IL-12 and IFN-γ promote the differentiation of naive $CD4^+$ T cells into Th1 cells[13]. Conversely, TGF-β can inhibit Th1 differentiation while promoting the differentiation into Th2 cells alongside IL-4[14]. The regulation of Th17 cells is even more intricate, involving a network of cytokines including IL-1β, IL-6, TGF-β, and IL-23, as well as Tregs[15].

In our study, aPD-L1 NVs@cGAMP exerts its effects by blocking PD-L1 and activating the STING pathway in various cells. Both PD-L1 blockade and STING pathway activation lead to increased activation and proliferation of T cells, resulting in elevated secretion of IFN-γ[16, 17, 18]. Importantly, STING agonists can also activate dendritic cells and macrophages, prompting them to secrete substantial amounts of IL-12[16]. The elevation of these cytokines effectively promotes the differentiation of naïve $CD4^+$ T cells into Th1 cells. Moreover, activation of the cGAS-STING pathway by aPD-L1 NVs@cGAMP leads to the production of substantial amounts of type I interferons and other pro-inflammatory cytokines. These factors can inhibit the TGF-β signaling pathway in Tregs, M2 macrophages, and cancer-associated fibroblasts (CAFs), ultimately reducing the secretion of TGF-β[19, 20]. Decreased TGF-β levels in the TME reduce the differentiation of naïve $CD4^+$ T cells into Th2 cells. Under these combined influences, $CD4^+$ T cells in the TME are more inclined to differentiate into Th1 rather than Th2 cells. The reduction in Th2 cells leads to

decreased IL-4 secretion, further diminishing Th2 cell numbers. Additionally, the pro-inflammatory environment characterized by elevated IL-6 and reduced TGF-β levels can supports the upregulation of Th17 cells[15]. The increased Th17 cells can recruit other immune cells to the TME, enhancing the antitumor immune response.

Therefore, the observed changes in Th1, Th2, and Th17 cell populations are likely due to the combined effects of PD-L1 blockade, increased pro-inflammatory cytokines (such as IFN-γ, type I interferons, and IL-6), and decreased TGF-β levels induced by aPD-L1 NVs@cGAMP treatment.

We have incorporated this discussion into the revised manuscript, as follows:

"The increased Th1/Th2 ratio may be directly associated with PD-L1 blockade, elevated IFN-γ levels, and decreased TGF-β levels induced by aPD-L1 NVs@cGAMP. PD-L1 blockade and increased IFN-γ can promote the differentiation of naive $CD4^+$ T cells into Th1 cells, whereas reduced TGF-β levels can inhibit the differentiation into Th2 cells. Furthermore, the upregulation of Th17 cells may be directly associated with the increased IL-6 levels and the pro-inflammatory microenvironment induced by aPD-L1 NVs@cGAMP. "

We appreciate your valuable suggestion, which has helped us clarify these results and improve our manuscript.

Q: Minor comments：*1.* Please complete the unit information for the in vivo imaging figures.

R: Thank you for your valuable suggestion. Per your suggestion, we have added the appropriate unit information to all the *in vivo* imaging figures in the manuscript and corrected any inaccuracies.

Q: *2.* The image data and corresponding statistical data are not presented together, making it difficult to read. The authors need to rearrange the layout of the images.

R: Thank you for your constructive feedback. In response, we have reorganized the layout of the figures in our manuscript, particularly focusing on **Figure 5**. The image data and the corresponding statistical analyses are now presented together.

Q: *3.* Please complete the statistical analysis of Supplementary Figure 12b, d, f.

R: Thank you for your valuable suggestion. In response, we have performed and included the statistical analyses for **Supplementary Figures 12b, 12d, and 12f** in the revised manuscript.

Reviewer #4 *(Remarks to the Author):*

Q: *The revised manuscript by Zhu et al titled "Enhanced CAR-T cell activity against solid tumors by inhalable engineered nanovesicles" has extensively addressed to all the reviewers comments with a large number of additional experiments and with appropriate review of the previous literature to convincingly explain the*

background information needed for justifying the reviewers concerns. I am happy with the revision and can be now considered for publication.

R: Thank you very much for your positive feedback and recognition of our work.

References

1. Zhang X, Hartmann P. How to calculate sample size in animal and human studies. *Front Med (Lausanne)* **10**, 1215927 (2023).

2. Charan J, Kantharia ND. How to calculate sample size in animal studies? *J Pharmacol Pharmacother* **4**, 303-306 (2013).

3. Schmidt SAJ, Lo S, Hollestein LM. Research Techniques Made Simple: Sample Size Estimation and Power Calculation. *J Invest Dermatol* **138**, 1678-1682 (2018).

4. Labanieh L, *et al.* Enhanced safety and efficacy of protease-regulated CAR-T cell receptors. *Cell* **185**, 1745-1763 e1722 (2022).

5. Ma L, *et al.* Vaccine-boosted CAR T crosstalk with host immunity to reject tumors with antigen heterogeneity. *Cell* **186**, 3148-3165 e3120 (2023).

6. Arifin WN, Zahiruddin WM. Sample Size Calculation in Animal Studies Using Resource Equation Approach. *Malays J Med Sci* **24**, 101-105 (2017).

7. Zhao Y, *et al.* IL-10-expressing CAR T cells resist dysfunction and mediate durable clearance of solid tumors and metastases. *Nat Biotechnol* **42**, 1693-1704 (2024).

8. Larson RC, *et al.* CAR T cell killing requires the IFNgammaR pathway in solid but not liquid tumours. *Nature* **604**, 563-570 (2022).

9. Lim RJ, *et al.* CXCL9/10-engineered dendritic cells promote T cell activation and enhance immune checkpoint blockade for lung cancer. *Cell Rep Med* **5**, 101479 (2024).

10. House IG, *et al.* Macrophage-Derived CXCL9 and CXCL10 Are Required for Antitumor Immune Responses Following Immune Checkpoint Blockade. *Clin Cancer Res* **26**, 487-504 (2020).

11. Harlin H, *et al.* Chemokine expression in melanoma metastases associated with CD8+ T-cell recruitment. *Cancer Res* **69**, 3077-3085 (2009).

12. Basu A, *et al.* Differentiation and Regulation of T(H) Cells: A Balancing Act for Cancer Immunotherapy. *Front Immunol* **12**, 669474 (2021).

13. Dong C. Cytokine Regulation and Function in T Cells. *Annu Rev Immunol* **39**, 51-76 (2021).

14. Golubovskaya V, Wu L. Different Subsets of T Cells, Memory, Effector Functions, and CAR-T Immunotherapy. *Cancers (Basel)* **8**, (2016).

15. Guery L, Hugues S. Th17 Cell Plasticity and Functions in Cancer Immunity. *Biomed Res Int* **2015**, 314620 (2015).

16. Li G, *et al.* cGAS-STING pathway mediates activation of dendritic cell sensing of immunogenic tumors. *Cell Mol Life Sci* **81**, 149 (2024).

17. Liu S, Verma A, Kettenberger H, Richter WF, Shah DK. Effect of variable domain charge on in vitro and in vivo disposition of monoclonal antibodies. *MAbs* **13**, 1993769 (2021).

18. Chin EN, Sulpizio A, Lairson LL. Targeting STING to promote antitumor immunity. *Trends Cell Biol* **33**, 189-203 (2023).

19. Yi M, *et al.* Targeting cytokine and chemokine signaling pathways for cancer therapy. *Signal Transduct Target Ther* **9**, 176 (2024).

20. Li C, Jiang P, Wei S, Xu X, Wang J. Regulatory T cells in tumor microenvironment: new mechanisms, potential therapeutic strategies and future prospects. *Mol Cancer* **19**, 116 (2020).

Point-by-Point Response

NOTE: The comments are in italic black font, and our responses are in normal blue font. "Q" is short for "Question" and "R" is short for "Response".

Response to Comments from Reviewers

Reviewer #3 (Remarks to the Author):

***Q:** The authors have addressed my points adequately.*

R: Thank you very much for your positive feedback and recognition of our work.